Chem Soc Rev

REVIEW ARTICLE

View Article Online
View Journal | View Issue

Cite this: *Chem. Soc. Rev.*, 2026, **55**, 4756

Hidden interfacial electric fields in chemistry: contact electrification and beyond

Shaoxin Li,[abc] Zhong Lin Wang [a] and Di Wei *[ad]

A wide range of chemical transformations proceed at immiscible boundaries, including solid dielectric–liquid, gas–liquid, and liquid–liquid interfaces, even in the absence of light, heat or externally applied potentials. At these boundaries, intense interfacial electric fields emerging from interfacial charge transfer, molecular orientation, and asymmetric charge distributions can profoundly reshape reaction free-energy landscapes. Especially at solid dielectric–liquid interfaces, contact electrification (CE) mainly drives electron transfer, generating substantial surface charge densities and interfacial electric fields that critically govern radical formation and redox chemistry. Gas–liquid or immiscible liquid–liquid interfaces, exemplified by microdroplet reactions, as well as processes at biomolecular condensate-solution boundaries, exhibit intrinsic fields on the order of $\sim 10^6$–10^9 V m^{-1}. Notwithstanding the burgeoning interest in this area, further fundamental scrutiny is necessary to establish a unified conceptual framework for interfacial electric field-driven reactions, moving beyond empirical observations toward predictive control. In this review, interfacial electric fields are described as emerging from cooperative effects, including CE, oriented water dipoles and ion redistribution, while their dynamic fluctuations are highlighted as a critical factor in driving interfacial chemical reactions. Mechanical excitation, material electronegativity, solvent structure, ionic strength, pH and dissolved gases are discussed as key parameters that modulate these fields and the resulting reactivity. We further emphasize some open questions concerning their spatial distribution, temporal dynamics and reaction-driven evolution and highlight the need for advanced operando techniques capable of resolving interfacial electric fields with nanometer spatial resolution and sub-microsecond temporal resolution to establish causal links between electric field dynamics and reaction outcomes. Overall, interfacial electric fields emerge as hidden forces with far-reaching implications and should be elevated from passive boundary conditions to explicit design parameters for sustainable, high-efficiency interfacial chemistry.

Received 15th December 2025

DOI: 10.1039/d5cs01066g

rsc.li/chem-soc-rev

1. Introduction

The intrinsic relationship between charge and chemical reactivity, described by $\Delta G = -n$FE, establishes a fundamental link among Gibbs free energy, cell potential, and reaction spontaneity, forming the foundation of electrochemistry.[1] Since Faraday's pioneering work, electrochemistry has served as a bridge connecting electricity with chemical transformations.[2,3] Importantly, electrostatic fields have been shown to influence catalytic activity, highlighting that interfacial electric fields beyond externally applied potentials can govern chemical reactivity.[4] Arieh Warshel proposed an electrostatic contribution to catalysis, suggesting that the polarity of the active sites in enzymes, which was overlooked for decades, plays a critical role in reaction energetics.[5] This idea was supported experimentally in 2014, when Boxer *et al.* demonstrated a link between charge anisotropy in enzymes and chemical catalysis.[6] Besides, Li *et al.* indicated that a strong electrostatic field exists in the molecular-scale space of zeolites due to the charge distribution in the zeolite framework, which has a significant impact on the potential energy of guest molecules and their activation.[7] Zeolitic spatial constraints and local electric fields cooperatively modulate chemical reactivity, establishing intrinsic electrostatics as a foundational pillar of catalysis. This extends electrochemical principles to the molecular scale, where autonomous interfacial electric fields replace the need for externally applied potentials.

In this context, contact electrification (CE) has emerged as a powerful mechanism for driving chemical transformations on triboelectrically charged solid dielectric surfaces. Achieving a detailed understanding of CE at heterogeneous interfaces is

[a] *Beijing Institute of Nanoenergy and Nanosystems, Chinese Academy of Sciences, Beijing 101400, P. R. China. E-mail: weidi@binn.cas.cn*
[b] *School of Nanoscience and Engineering, University of Chinese Academy of Sciences, Beijing 100049, P. R. China*
[c] *Department of Chemistry, Stanford University, Stanford, California 94305, USA*
[d] *Centre for Photonic Devices and Sensors, University of Cambridge, 9 JJ Thomson Avenue, Cambridge, CB3 0FA, UK*

critical for elucidating charge-transfer kinetics and guiding the rational design of interfacial reactions. In a pioneering study, Liu and Bard demonstrated that CE on polytetrafluoroethylene (PTFE) surfaces can generate highly energetic electrons capable of reducing metal ions and triggering electrochemiluminescence reactions.[8] Extending this concept, Zhang and colleagues showed that luminol droplets exhibit distinct chemical behaviors depending on the charge polarity induced by CE with different solid dielectrics.[9] Luminol droplets acquiring positive charge through CE with PTFE exhibited enhanced reactivity and intensified chemiluminescence, whereas negatively charged droplets *via* CE with nylon displayed suppressed luminescence. These results underscore the critical influence of the net charge polarity of droplets by CE with a solid dielectric on chemical reactivity, positioning CE as a central factor in controlling reaction outcomes. In recent years, contact-electro-catalysis (CEC) has emerged as a transformative strategy that exploits triboelectric charge transfer driven by CE at solid dielectric–liquid interfaces to initiate and accelerate chemical reactions.[10] This approach harnesses CE-induced interfacial charges as a clean and sustainable driving force, offering new opportunities for catalytic innovation, such as pollutant degradation, hydrogen peroxide (H_2O_2) generation and ammonia synthesis.[10–12] The scope of CEC has further expanded to the environmentally benign recovery of cathode materials from spent lithium-ion batteries, achieving high leaching efficiencies for cobalt and lithium under mild, acid-free conditions.[13] Building on these advances, our previous works extended CE-driven chemical processes to a broad spectrum of chemical transformations, including contact-electro-redox reactions of $[Fe(CN)_6]^{3-}$/$[Fe(CN)_6]^{4-}$, contact-electro-polymerization of aniline, contact-electro-fluorescence of terephthalic acid, and contact-electro-luminescence of luminol.[14–16] Collectively, these studies establish a unifying framework, contact-electro-chemistry (CE-Chemistry),[14] which has also been successfully demonstrated in non-aqueous media such as dimethyl sulfoxide (DMSO).[17] Regarding the Janus nature of CE-Chemistry systems, in which both oxidative and reductive reactions can occur, we further demonstrated that the redox selectivity is dictated by the standard electrode potentials (SEPs) of the reactive species, establishing a threshold that determines whether oxidative or reductive pathways predominate.[18] These findings underscore that CE extends beyond a mere physical phenomenon of charge transfer, actively promoting interfacial chemical reactivity and motivating further mechanistic investigations into its relationship with interfacial electric fields.

Alternatively, a growing body of evidence demonstrates that gas–liquid interfaces, particularly those in microdroplet systems, can intrinsically promote a wide range of chemical transformations, including addition, elimination and redox

Shaoxin Li

Shaoxin Li received her PhD degree in Materials Science from the University of Chinese Academy of Sciences in 2022. She is a postdoctoral researcher at the same university and she currently a visiting postdoctoral researcher at Stanford University. Her research focuses on contact electrification, contact electrochemistry, self-powered sensors/systems.

Zhong Lin Wang

Zhong Lin Wang received his PhD degree in Physics from Arizona State University. He is the Director of the Beijing Institute of Nanoenergy and Nanosystems and a Regents' Professor and Hightower Chair at the Georgia Institute of Technology. He pioneered the field of nanogenerators for distributed energy, self-powered sensors, and large-scale blue energy. He coined the fields of piezotronics and piezo-phototronics for third-generation semiconductors. His Google Scholar citation count is over 400 000, with an h index of over 300.

Di Wei

Di Wei received his PhD degree in Electrochemistry from Åbo Akademi University. He is a Principal Investigator at the Beijing Institute of Nanoenergy and Nanosystems and leads the Iontronics Laboratory. He is a Fellow of multiple international academies and societies, including FEurASc, MEASA, FNAI (USA), FRSC and FIMMM, and a Life Senior Member of Wolfson College, University of Cambridge. He has authored over 140 papers in leading journals (Nature Energy, Nature Communications, JACS, Joule, Advanced Materials, Angewandte Chemie, etc.) and holds more than 200 international patents, many of which have been transferred to industry including Nokia and Lyten. His work has been recognized by the Nokia Global Innovation and Excellence Award and the ISE Brian Conway Prize, and he is listed among the top 2% of global scientists (Stanford-Elsevier).

reactions, even in the absence of catalysts and externally applied electric fields.[19–30] These observations underscore the intrinsic chemical reactivity of interfacial environments.[31–33] Processes such as hydrogen–deuterium exchange and protein folding–unfolding have been shown to proceed markedly faster at microdroplet interfaces than in bulk solution.[34] In mechanistic interpretations, microdroplet reactivity has been attributed to a combination of partial solvation, preferential molecular orientation, extreme interfacial acidity or basicity, rapid solvent and reagent evaporation, and the presence of strong local interfacial electric fields.[30,34–40] Recent studies indicate that the emergent interfacial properties of water originate from its propensity to acquire charge during common physicochemical processes, including evaporation, condensation, spraying, splashing and crystallization.[30,41] Although the mechanistic origins of microdroplet-accelerated chemistry remain under active investigation owing to the complexity of droplet interfaces, intense interfacial electric fields have emerged as a particularly compelling driver of microdroplet reactivity.[42] At the molecular scale, interfacial electric fields along free O–H bonds at air–water interfaces have been estimated to reach $\sim 1.6 \times 10^9$ V m^{-1}, far exceeding those within the droplet interior.[43] Using stimulated Raman-excited fluorescence microscopy with nitrile-based Stark probes, interfacial electric fields at water–oil microdroplet boundaries have likewise been quantified to be $\sim 10^9$ V m^{-1}.[44] Analogously, in biomolecular condensates formed by liquid–liquid phase separation, ion partitioning and charge asymmetry between dense and dilute phases generate interfacial electric fields on the order of $\sim 5 \times 10^6$ V m^{-1}, which are sufficient to actively promote chemical reactions.[45] Collectively, interfacial electric fields may profoundly influence by electron transfer, ion redistribution and molecular orientation at phase boundaries. Critically, these interfaces may permit large electric field fluctuations, giving rise to Lorentzian distributions of local electric field strengths that can transiently reach values sufficient to modulate reactivity.[30,43,46,47] Thus, this dynamic electric field heterogeneity constitutes a concealed driving force capable of initiating chemical transformations.

In this context, we place particular emphasis on the critical role of interfacial electric fields, especially from the perspective of CE, which can regulate interfacial electron transfer, ion redistribution, and the resulting electric field strength and dynamics. These coupled processes exert a sustained and profound influence on the recently emerging CE-Chemistry paradigm. Moreover, interfacial electric fields at gas–liquid and immiscible liquid–liquid interfaces are also considered, as growing evidence suggests that they can likewise accelerate and bias chemical reactions. These emerging insights point to a broader conceptual shift in interfacial chemistry, where interfacial electric fields are not passive by-products of contact, but active energetic contributors that reshape reaction pathways. Deciphering and harnessing these interfacial electric fields may open new avenues for interfacial chemistry and sustainable catalysis.

2. Hidden interfacial electric fields at solid–liquid interfaces

An interfacial electric field is generally defined as the negative gradient of a spatially varying electrostatic potential.[48] In the classical picture derived from Coulomb's law, the electrostatic potential is obtained as the superposition of contributions from all point charges, and the corresponding electric field follows as its spatial gradient. In continuum treatments, this description is cast into Poisson's equation, $\nabla^2\varphi = -\rho/\varepsilon$, where φ is the electrostatic potential and ε the dielectric constant. However, both Coulombic and Poisson-based formulations neglect a crucial molecular-level effect, the local environmental response to a charged species.[48] Recent molecular dynamics simulations further reveal that electrode–liquid interfaces host intense, structurally encoded interfacial electric fields that are largely inaccessible to classical continuum theory.[49] In these systems, interfacial electric field profiles are obtained from microscopic models that prescribe the detailed shape of the potential across the interface (Fig. 1a). A growing body of studies has converged on the view that interfacial electric fields play an active and often decisive role in electrochemistry. They demonstrated that interfacial electric field amplification arising from nanoscale confinement,[50,51] interfacial polarization,[52] or charge accumulation can reshape local electronic structures,[53,54] lower activation barriers, and steer reaction pathways.[55] These effects have been exploited across applications, such as CO_2 reduction[56,57] and catalysis,[58] underscoring interfacial electric fields as a general and designable driving force in interfacial chemistry.

Strikingly, even under a zero applied bias, a finite intrinsic interfacial potential persists because interfacial water molecules spontaneously orient their dipoles toward the surface, generating a built-in electrostatic environment that eludes conventional mean interfacial electric field descriptions.[59] The resulting interfacial electric fields are not smoothly screened but instead exhibit large magnitudes, rapid temporal fluctuations, and pronounced spatial oscillations on molecular length scales.[60] Both cations and anions experience net repulsive fields near the interface, and electric field fluctuations intensify away from the surface despite electrostatic screening. Collectively, these observations establish that electrode–liquid interfaces are governed not by a single deterministic potential, but by a fluctuation-dominated electrostatic microenvironment in which hidden interfacial electric fields arise spontaneously from molecular organization, persist without an external bias, and continuously regulate charge transport and reaction dynamics.[61] Interfacial potentials arising spontaneously at functional interfaces transcend the classical electrode–aqueous electrolyte paradigm. For instance, at solid–liquid interfaces, the interfacial electric field stems predominantly from surface charges or dipoles of the solid, inducing instantaneous counterion adsorption from the ionic liquid and resulting in a compact, Helmholtz-type monolayer structure.[62] The absence of solvent molecules and the ultrahigh ionic concentration in ionic liquids render classical double-layer models inadequate and Debye–Hückel screening inapplicable,[63,64] thus necessitating

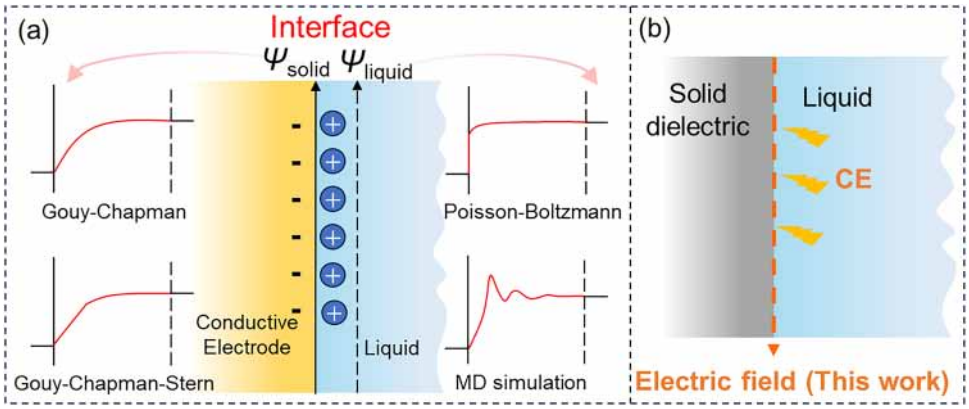

Fig. 1 Interfacial electric field at the solid–liquid interface. (a) Representative models used to predict distinct interfacial electric field profiles. (b) Interfacial electric field from the solid dielectric–liquid CE.

theoretical frameworks that incorporate strong ion correlations and overscreening effects.[65,66] Furthermore, at the soda-lime glass-water interface, Na^+ leaching coupled with H^+ ingress leads to the formation of a hydrated, negatively charged silica-rich layer. Ion partitioning across this fixed-charge interphase generates a Donnan potential, and thus a localized electric field, without any externally applied bias.[67]

The interfacial electric field extends well beyond the realm of equilibrium electrostatics. When solid dielectrics come into contact with liquids, they readily accumulate electrical charge through the ubiquitous CE process, resulting in spontaneously generated non-equilibrium interfacial potentials. Scientific interest in charge-transfer mechanisms across solid dielectric–liquid boundaries has persisted for several decades. A foundational study conducted in the 1980s by El-Kazzaz and Rose-Innes demonstrated that contacting liquid metals with insulating dielectric substrates could induce measurable surface charging.[68] Subsequent investigations expanded this observation to aqueous systems, revealing that mere contact between water and dielectric surfaces, such as polymers, can generate substantial surface charge.[69,70] Nevertheless, the identity of the charge-carrying species responsible for transfer in aqueous environments remains unresolved. Despite extensive experimental and theoretical work, the origin of charge carriers (electrons *versus* ions) and their transport pathways in solid dielectric–liquid CE continue to be actively debated. This section summarizes the current mechanistic understanding of solid dielectric–liquid CE, covering electron transfer, ion migration, and interfacial electrical double layer (EDL) formation. Within this framework, the recent research by our group on triboelectrically regulated EDL formation at solid dielectric–liquid dielectric interfaces,[71–74] conceptually analogous to electrochemical EDL, suggests that a localized interfacial electric field (Fig. 1b) may arise from the CE process. This electric field holds the potential to drive interfacial redox reactions without an external bias or conventional catalytic inputs.

2.1. Electric fields induced from solid dielectric–liquid CE

For solid dielectric–water interfaces, surface charging has long been attributed predominantly to ion-transfer processes, although the underlying microscopic picture remains incomplete. In this classical framework, interfacial charge is thought to arise either from the selective adsorption of solution ions, such as OH^- and H^+, onto the dielectric surface,[70,75] or from the dissociation of surface functional groups intrinsic to the solid matrix.[76,77] A representative example is PTFE, which under neutral or alkaline conditions preferentially binds OH^- and H^+ over other electrolyte species.[78] This selectivity toward OH^- has been ascribed to its relatively weak hydration and favorable hydrogen-bonding interactions with interfacial water.[79] However, an ion-adsorption-only model becomes insufficient in scenarios where charge exchange proceeds in the absence of dissociated ions, such as at interfaces between solid dielectrics and non-aqueous liquids, including oils that also acquire charge upon contact.[80] These observations imply the existence of additional interfacial charge-transfer pathways beyond simple ion adsorption, thereby motivating continued efforts to elucidate the fundamental mechanism of solid dielectric–liquid CE. Beyond this classical picture, Wang *et al.* demonstrated that models assuming that CE at the PTFE–water interface is driven solely by OH^- transfer underestimate the charge density by more than an order of magnitude, indicating that ion transfer alone cannot account for the observed effects; instead, electron transfer contributes approximately 90% of the interfacial charge-generation in deionized water.[81] Subsequently, they further revealed that electrons preferentially transfer from water molecules to the PTFE surface during CE. This behavior can be rationalized in terms of a transient intermolecular electron-cloud overlap mechanism, whereby intimate interfacial contact enables transient electronic coupling and charge transfer.[82] As illustrated in Fig. 2a(i), the outer-shell electrons of oxygen in water reside in a potential well, whereas the lowest unoccupied molecular orbital (LUMO) of PTFE serves as an efficient electron acceptor. Prior to contact, electrons are localized within their respective wells (Fig. 2a(ii)); upon contact, electrons transfer from water to the PTFE LUMO, reaching a lower-energy equilibrium state (Fig. 2a(iii)). During subsequent separation, the accumulated negative charges on PTFE become exposed at the interface,

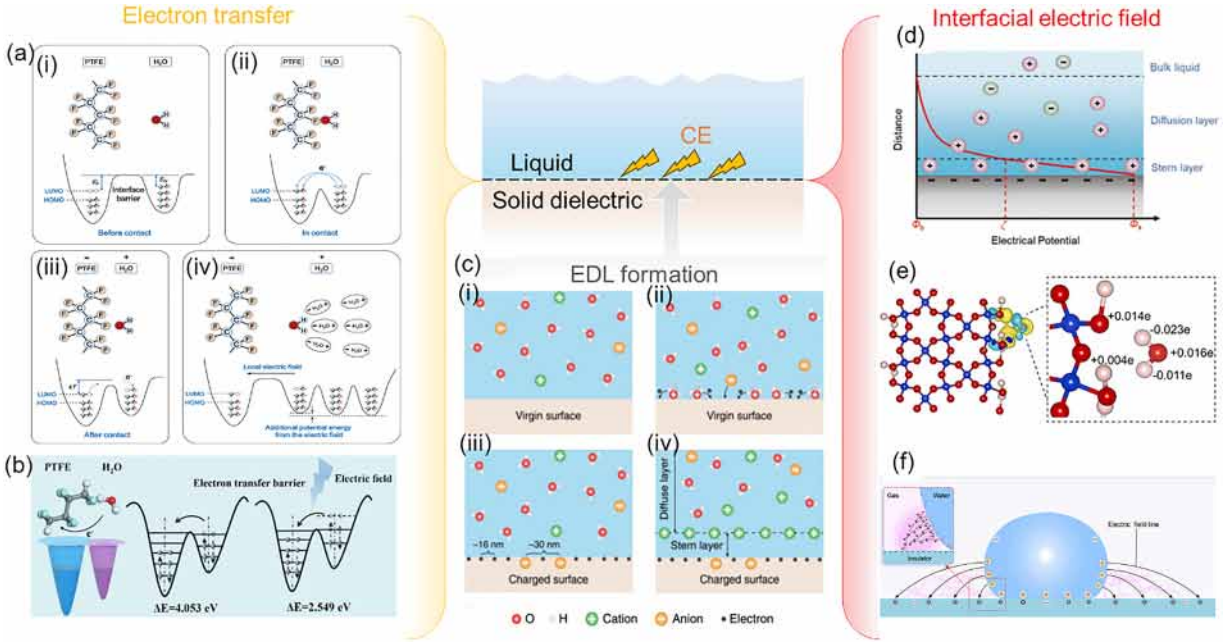

Fig. 2 Theoretical insights into the solid dielectric–liquid CE. (a) Schematic of electron transfer between water and PTFE: (i) before contact, (ii) during contact, (c) after contact upon separation, and (iv) after separation with a new equilibrium state. Reproduced from ref. 81 with permission from John Wiley and Sons, copyright 2019. (b) CEC *via* electret behavior facilitating interfacial electron transfer. Reproduced from ref. 90 with permission from the American Chemical Society, copyright 2024. (c) Proposed mechanism of solid dielectric–liquid CE and formation of the EDL: (i) before CE, (ii) electron transfer between the water and the virgin surface during CE, (iii) generation of ions at the electrical charged surface, and (iv) migration of opposite charged ions toward the surface, electrically screening the first charged layer. Reproduced from ref. 83 with permission from Springer Nature, copyright 2020. (d) Electric potential distribution at the CE interface between water and a solid dielectric. Reproduced from ref. 88 with permission from John Wiley and Sons, copyright 2020. (e) Electron density difference between SiO_2 with a single H_2O molecule, with the number of electrons gained and lost marked on the corresponding atoms. Reproduced from ref. 89 with permission from Elsevier, copyright 2023. (f) Electrostatic breakdown at solid dielectric–liquid–gas triple-phase interfaces induced by CE. Reproduced from ref. 91 with permission from Elsevier, copyright 2025.

generating a localized electric field (Fig. 2a(iv)). Unlike metallic electrodes where charge redistribution is governed by the bulk Fermi level, solid dielectric–liquid interfaces rely on localized electronic states. Recent *ab initio* simulations of an insulating solid dielectric interacting with water reveal that charge transfer is mediated by surface states, localized energy levels introduced by surface defects, dangling bonds, or functional groups.[83] Electron localization function and Bader charge analysis were used to provide the first atomistic evidence that solid dielectric–liquid CE is driven by electron cloud overlap and subsequent electron transfer. This effectively bridges the gap between the macroscopic hidden fields and the microscopic electronic structure.[84] Thus, for inert fluorinated dielectrics such as PTFE and FEP, the CE process establishes an electric field arising from trapped electrons, which perturbs the electronic structure of the dielectric by modulating the energies of its LUMO and highest occupied molecular orbital (HOMO)[85] (Fig. 2b).

Advances in the mechanistic understanding of CE at solid dielectric–liquid interfaces have driven a paradigm shift beyond conventional electrochemical EDL models, establishing electron transfer as a central determinant of the interfacial insulating structure. Within this emerging framework, electrons and ions jointly constitute a composite Stern layer. Wang *et al.* proposed a hybrid EDL model based on a two-step process that couples interfacial electron transfer with subsequent ion adsorption.[83] In the initial stage (Fig. 2c(i)), water molecules and solvated ions (*e.g.*, H_2O, cations and anions) are driven toward the pristine solid dielectric surface by thermal motion and hydrodynamic pressure (Fig. 2c(ii)). During these interfacial collisions, transient overlap between the electronic clouds of water molecules and surface atoms enables interfacial electron exchange (Fig. 2c(ii)),[82] while concomitant surface ionization processes may also occur. As a consequence, both electrons and ionic species are generated at the interface (Fig. 2c(iii)). In the second stage, following charge separation, free counter-ions in the liquid migrate toward the charged surface under electrostatic attraction, thereby establishing an EDL (Fig. 2c(iv)). Notably, counter-ions from the liquid phase do not remain rigidly immobilized on the triboelectrically charged surface. Instead, thermal fluctuations sustain their continuous motion within the interfacial region, giving rise to a concentration gradient characterized by counter-ion enrichment near the charged surface and co-ion depletion (Fig. 2d).[86–88] An atomic-level investigation on the effect of CE on the solid dielectric–liquid EDL were performed *via* first-principles and molecular dynamics (MD) simulations. Their results suggest that this CE can influence the distribution of ions in the solution, thus influencing the formation of the EDL, and even reversing its polarity under a specific surface charge density (Fig. 2e).[89] Moreover, space-charge-

induced interfacial electric fields can reshape the dielectric band structure and exert strong electrostatic forces at solid dielectric–water interfaces, thereby promoting interfacial carrier transfer.[90] Ye *et al.* further demonstrated that charge transfer at solid dielectric–water interfaces can reach extreme magnitudes, frequently giving rise to electrostatic breakdown at the solid–liquid–gas triple-phase boundary, where localized interfacial electric fields in the gas phase are strongly amplified (Fig. 2f).[91] Building on this solid dielectric–liquid CE framework, our group has exploited the resulting EDL to enable nanoscale ionic–electronic coupling, allowing precise regulation of ion transport and interfacial electric fields.[71] Dynamic modulation *via* mechanical, electrostatic or triboelectric-induced ion polarization offers versatile strategies to enhance both energy harvesting[92] and information transduction.[74,93–95] Collectively, these findings underscore the profound and highly tunable interfacial electric fields intrinsic to solid dielectric–liquid CE.

2.2. CE-Chemistry

2.2.1. Role of triboelectric charges. Triboelectric charges generated by CE are increasingly recognized as active chemical actors rather than passive electrostatic artefacts. Early studies established that dielectrics pre-charged by solid–solid CE can subsequently function as self-biased single electrodes upon immersion in solution, thereby enabling spontaneous redox reactions without external wiring or applied potential. In a seminal contribution, Liu *et al.* applied Faraday's law to quantify surface charge density and demonstrated the pivotal role of electron transfer in chemical reactions driven by triboelectrically charged polymers.[8] Using a triboelectrically charged polymer as a single electrode, they induced diverse solution-phase reactions, including pH modulation, hydrogen evolution, and metal-ion reduction.[96,97] For example, after rubbing Teflon with Plexiglas, the charged Teflon was immersed in a $CuSO_4$ solution, where it directly drove the reduction of Cu^{2+}.[8] Energy-dispersive X-ray spectroscopy (EDS) confirmed the formation of metallic Cu on the Teflon surface, with Cu signals uniformly detected at all the examined sites, while no Cu was observed on the uncharged Teflon. Optical absorbance measurements of the $CuSO_4$ solution before and after contact further substantiated the reduction of Cu^{2+} (Fig. 3a). The observed concentration change corresponded to an average surface charge density of $\sim 8 \times 10^{14}$ cm^{-2} (based on geometric area), in close agreement with values independently inferred from pH variation. Analogous behaviour was observed for the reduction of $[Fe(CN)_6]^{3-}$ to $[Fe(CN)_6]^{4-}$, which proceeded only in the presence of triboelectrically charged Teflon. Moreover, immersion of CE-charged polymethylmethacrylate (PMMA), generated by contact with polyethylene (PE), into an acetonitrile/H_2O solution containing $[S_2O_8]^{2-}$ and $[Ru(bpy)_3]^{2+}$ produced a sharp rise in chemiluminescence intensity, directly correlating the fluorescence enhancement with the surface triboelectric charge on the polymer.[97] The quantitative application of Faraday's law in these studies explicitly established the central role of electron

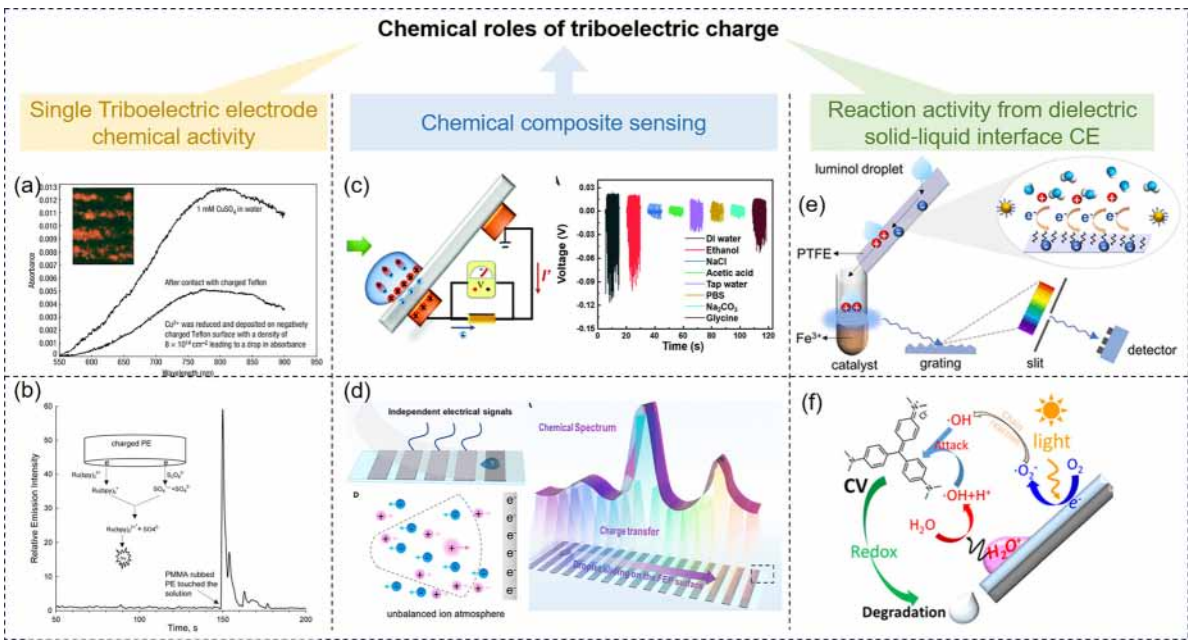

Fig. 3 Chemical roles of triboelectric charge. (a) Optical absorbance of 1 mM $CuSO_4$ solution before and after contact with charged Teflon. Reproduced from ref. 8 with permission from Springer Nature, copyright 2008. (b) Device design and performance of CEC CO_2RR. Reproduced from ref. 100 with permission from Springer Nature, copyright 2024. (c) Self-powered liquid chemical sensors based on the solid dielectric–liquid CE. Reproduced from ref. 105 with permission from the Royal Society of Chemistry, copyright 2021. (d) Triboelectric charge generation at the solid dielectric–liquid interfaces for chemical analysis. Reproduced from ref. 107 with permission from the American Chemical Society, copyright 2024. (e) Electrostatic charge-regulated chemiluminescence *via* interfacial electron-transfer at solid dielectric–liquid interfaces. Reproduced from ref. 9 with permission from the American Chemical Society, copyright 2022. (f) Insulating polymers enable efficient visible-light catalysis through CE. Reproduced from ref. 108 with permission from Elsevier, copyright 2022.

transfer in triboelectrically charged insulating solids. Subsequent investigations refined this mechanistic picture by disentangling the relative roles of static charge magnitude and surface charge chemistry.

Zhang *et al.* demonstrated that the amount of metal deposited on triboelectrically charged polymer surfaces scales nearly linearly with surface charge density, with the proportionality coefficient governed by the stability of anionic surface charge carriers.[98] This result implies that the dominant driving force is not merely the stored electrostatic charge, but rather the intrinsic chemical reactivity of the surface-bound charge species. Accordingly, materials capable of stabilizing anionic carriers, through favorable electron affinity and ionization-energy alignments, support more extensive redox chemistry, whereas dielectrics with less stable anions are better suited for delivering small, precisely metered redox inputs. Consistently, Chamberlayne *et al.* provided a rigorous thermodynamic analysis demonstrating that the electrostatic contribution to the Gibbs free energy is fundamentally capped, reaching at most the thermal voltage ($\sim$25.7 mV in monovalent aqueous electrolytes at 25 °C).[99] Li *et al.* demonstrated that CE between poly(vinylidene fluoride) PVDF/single-Cu-atom-anchored polymeric carbon nitride (Cu-PCN) and quaternized cellulose nanofibers (CNF) can directly initiate CO_2 reduction in ambient air, where triboelectric nanogenerator (TENG)-driven electron transfer forms CO_2^- intermediates that evolve into CO under humid conditions (Fig. 3b).[100] Extending this approach, a dual Cu-PCN/CuO catalyst on an electronegative tribolayer delivered a faradaic efficiency of 63.5% toward C_2H_4 in dilute CO_2 owing to the high triboelectric charge density at 99% RH.[101] Kim *et al.* further used nanorod-patterned PPy electrodes to concentrate triboelectric charges for motion-powered electroporation, achieving >6-log pathogen inactivation in 500 mL of water within 10 min and robust cycling stability.[102]

Repeated contact-separation between solid dielectrics and water can lead to substantial surface charge accumulation, yielding interfacial potentials of up to $\sim$150 V.[103] Thus, triboelectrically charged surfaces function as chemically active interfaces, whose carrier stability, redox character, and electrolyte-dependent screening directly couple interfacial chemistry to electrical output. This coupling provides a mechanistic basis for triboelectric signal-coupled sensing architectures, in which analyte-induced modulation of surface charge and interfacial potential serves as a direct chemical and compositional readout. A foundational advance was reported by Gibson *et al.*, which is triboelectric charging can serve as a sensitive probe of surface chemistry.[104] Using cascaded metal beads and polymer films, they showed that both the magnitude and polarity of charge transfer correlate systematically with surface molecular structure. Although lacking molecular specificity, this approach enabled the detection of trace contamination, monolayer-level chemical modification, and even surface reaction kinetics, positioning triboelectric analysis as a low-cost, non-destructive, and highly responsive diagnostic tool. Building on this concept, Wang *et al.* developed self-powered triboelectric sensors for liquid-phase chemical analysis, in which solid dielectric–liquid CE provides the primary electrical signal.[105] A representative system employs a negatively charged PTFE film coupled with dual copper electrodes, where passing droplets induce coupled EDL release in the liquid and surface charge retention on the solid (Fig. 3c). The resulting characteristic positive and negative voltage spikes serve as chemical fingerprints. Systematic studies with amino acids (*e.g.*, glycine, lysine, and phenylalanine) revealed logarithmic scaling of negative voltage peaks with concentration, while investigations of organic and inorganic electrolytes demonstrated strong correlations between signal polarity/amplitude and free ion content. These observations indicate that multi-source interfacial charge-generation can produce binary-like electrical signatures directly reflecting liquid composition. These triboelectric sensors provide a low-cost, portable, and surface-charge-driven platform for chemical identification and quantification. Along similar lines, dual triboelectric signals generated at oil–water–solid multiphase interfaces have enabled a self-powered dual-signal platform for biochemical sensing, exemplified by dopamine detection.[106] More recently, Zhang *et al.* advanced this concept through the development of triboelectric spectroscopy, which integrates solid dielectric–liquid CE with surface charge-transfer for chemical analysis (Fig. 3d).[107] By monitoring triboelectric charges generated as liquids slide across solid surfaces, this approach achieves chemical identification with up to 93% accuracy and detection limits at the parts-per-billion level.

Building on droplet-based TENG concepts, Zhang *et al.* investigated triboelectrically charged luminol droplets interacting with solid dielectrics *via* solid dielectric–liquid CE.[9] The chemiluminescence was enhanced exclusively for positively charged luminol droplets, whereas negatively charged droplets suppressed light emission, providing direct evidence that electrons act as the primary charge carriers at the solid dielectric–liquid interface (Fig. 3e). This strategy enables the triboelectric modulation of chemiluminescence through static charging of reaction solutions and highlights key considerations for sample preparation in CE-Chemistry. Furthermore, CE between water droplets and PTFE generates abundant oxidizing radicals, while the concomitant electrical output enables *in situ* monitoring of catalytic activity (Fig. 3f).[108] Efficient carrier transport driven by mechanical forces and the widespread generation of reactive oxygen species (ROS) markedly accelerate dye degradation; crystal violet is degraded with 90% efficiency within 38 s, corresponding to a rate constant of 3.7 min^{-1}. Taken together, these advances establish triboelectric charge generated at solid dielectric–liquid interfaces as a versatile and previously underexplored modality for both chemical activation and molecular analysis.

2.2.2. From motion to reaction: mechanical activation of CE-Chemistry. The efficiency of CE can be governed by the characteristics of the mechanical stimulus, as mechanical motion directly dictates the frequency, duration, and quality of solid dielectric–liquid interfacial contact. Enhanced mechanical agitation accelerates interfacial renewal and promotes electron–cloud overlap between liquid molecules and solid dielectric surface atoms, thereby lowering the activation barrier

for interfacial electron transfer.[109] Accordingly, beyond simple droplet-sliding geometries, a diverse range of mechanically activated modes has been developed to amplify the CE performance in CE-Chemistry. As summarized in Fig. 4a, representative mechanical input strategies include continuous flow, magnetic stirring, ball milling, and ultrasonication. In flow-driven systems, liquid continuously contacts the inner surface of a dielectric channel, enabling sustained charge generation along the flow path and thereby supporting continuous reaction operation. Key parameters, including flow velocity, residence time, capillary length, and surface refresh rate, critically govern both triboelectric charge accumulation and the overall reaction efficiency. Jiang *et al.* demonstrated that hydroxyl radicals (·OH) can be generated when aqueous droplets interact with the inner walls of solid dielectric capillaries, even in the absence of any external energy input (Fig. 4b).[110] In their setup, droplets were continuously driven through long dielectric capillaries by nitrogen flow, producing repeated contact-separation events and thus flow-induced electrification. Using *o*-phenylenediamine (OPD) as an ·OH probe, which is oxidized to diaminophenothiazine (DAP) with a characteristic absorption at 424 nm, they confirmed radical formation in PTFE, silicone rubber, and nylon-6 capillaries. No DAP signal was detected in the control samples without capillary traversal, whereas all three dielectric materials produced distinct DAP absorption. The ·OH yield followed the trend PTFE > silicone rubber > nylon-6, directly correlating the radical-generation efficiency with the electron-withdrawing capability of the dielectric. These results establish that solid dielectric–liquid CE alone is sufficient to trigger ·OH formation from water and demonstrate the strong material-dependence of triboelectrically driven radical reactions. Building on the superior CE properties of FEP, the continuous degradation of methyl orange (MO) in a flow-electrification FEP tube was investigated.[15] As shown in Fig. 4c, a 0.01 mM MO solution was circulated through FEP tubes for 7 h, with periodic alcohol rinsing of the tube surface every hour to restore triboelectric charging. The progressive fading of the solution confirmed sustained MO degradation throughout long-term operation. Beyond conventional parameters such as inlet flow rate, tube inner diameter, and total length, we systematically evaluated different tubing network architectures. Under an identical total tube length and pump rotational speed, parallel

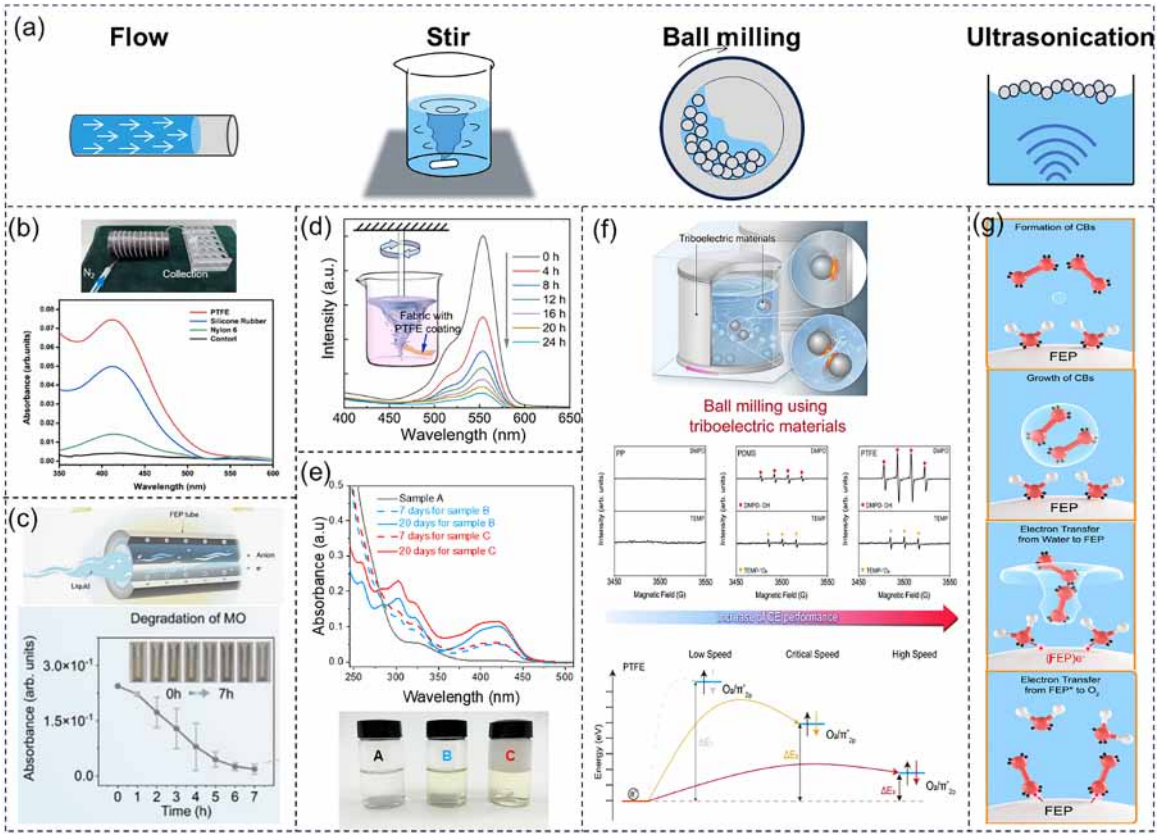

Fig. 4 Representative mechanical input strategies of CE-Chemistry. (a) Representative mechanical modes employed in CE-Chemistry. (b) Radical generation, reproduced from ref. 110 with permission from Elsevier, copyright 2023, and (c) MO degradation, reproduced from ref. 15 with permission from Elsevier, copyright 2024, induced by flow electrification at a solid dielectric–liquid interface. (d) Low-frequency CEC driven by friction between the PTFE-coated fabric and dye solution. Reproduced from ref. 111 with permission from Elsevier, copyright 2024. (e) Photograph and UV-vis spectra of $K_4[Fe(CN)_6]$ oxidation under stirring conditions *via* CE-Chemistry. Reproduced from ref. 14 with permission from Elsevier, copyright 2024. (f) CEC process for producing ROS *via* ball milling of triboelectric materials. Reproduced from ref. 112 with permission from Springer Nature, copyright 2024. (g) CEC process for producing ROS *via* ultrasound. Reproduced from ref. 10 with permission from Springer Nature, copyright 2022.

configurations consistently outperformed series arrangements, and increasing the number of parallel branches (*e.g.*, a five-branch network) further enhanced the degradation efficiency. This performance enhancement arises because parallel architectures reduce the flow velocity within each branch under a constant pump power, thereby extending the residence time and enabling more effective utilization of triboelectric charge accumulation along the solid dielectric–liquid interface.

Compared with continuous-flow configurations, mechanical stirring introduces more chaotic, multidirectional, and repetitive solid dielectric–liquid collisions within a confined volume, offering an alternative and highly effective route to activate CE-Chemistry. In a recent study, Jia *et al.* evaluated the CEC activity of PTFE-coated fabrics *via* the degradation of Rhodamine B (RhB) under overhead mechanical stirring.[111] As shown in Fig. 4d, the characteristic RhB absorption band at 554 nm decreased steadily during stirring in the dark, directly evidencing CE-Chemistry. The reaction efficiency exhibited a strong dependence on the stirring speed, where efficient RhB de-ethylation occurred only above ~800 rpm, whereas significantly diminished activity was observed at lower speeds, underscoring the necessity of sufficient frictional solid–liquid contact. Increasing both the stirring rate and PTFE loading further enhanced the catalytic performance, achieving ~91.5% RhB removal after 24 h at 1000 rpm using 1.1 g of PTFE-coated fabric. Consistently, in our previous work, continuous mechanical stirring of a $K_4[Fe(CN)_6]$ solution with a PTFE stir bar at 1500 rpm induced a gradual color change from colorless to green over 7 days, indicative of progressive CE-driven oxidation.[14] Accelerated oxidation was observed upon the addition of PTFE powder, which increased the effective solid dielectric–liquid interfacial area. As shown in Fig. 4e, the UV-vis spectra confirmed that a prolonged stirring time and enlarged dielectric contact area both promote the oxidation process, demonstrating that sustained mechanical stirring alone is sufficient to trigger CE-mediated redox reactions. Together, CE-Chemistry induced by continuous flow or mechanical stirring at solid dielectric–liquid interfaces represents a new reaction paradigm, enabling bias-free redox chemistry driven solely by mechanical energy. These findings challenge the long-standing assumption that hydrodynamic operations are chemically inert. Indeed, flow-based analytical platforms (*e.g.*, HPLC, flow injection analysis, and microfluidic devices), as well as routine stirring in synthetic chemistry, may inadvertently induce interfacial charge-transfer and radical formation, thereby influencing reaction pathways, kinetics, or analytical accuracy.

Beyond stirring and flow, ball milling, traditionally exploited in mechanochemistry and piezocatalysis, has recently been recognized as a powerful mechanical route to trigger CE-Chemical reactions. Using triboelectric polymer beads, Wang *et al.* demonstrated that repeated solid dielectric–liquid CE impacts during ball milling generate ROS capable of degrading organic pollutants (Fig. 4f).[112] Among polypropylene (PP), polydimethylsiloxane (PDMS), and PTFE, the latter exhibited the highest activity, consistent with its superior charge-trapping capability. A critical rotational speed was identified as the threshold mechanical energy (ΔE_2) required for interfacial electron transfer and radical generation, thereby establishing direct coupling between mechanical impact energy and CE-induced redox chemistry. At low milling speeds, the impact energy was insufficient to overcome the interfacial energy barrier (ΔE_1), resulting in negligible MO degradation. With increasing rotation speed, both the impact energy and the probability of electron transition increased, effectively lowering the kinetic barrier (ΔE_3) and accelerating radical production. These results establish a clear mechanochemical threshold for initiating CE-Chemistry and underscore the intimate coupling between mechanical energy input and interfacial electron-transfer dynamics.

Ultrasonication has emerged as one of the most effective and widely adopted strategies to enhance CE-Chemistry, owing to its simple operation, efficient energy delivery, and exceptional ability to activate solid dielectric–liquid interfaces. Wang *et al.* elucidated the mechanism by which ultrasonic irradiation promotes CE performance (Fig. 4g). During sonication, cavitation bubbles nucleate, grow, and collapse, generating intense microjets that repeatedly impact the solid surface. Upon impact, electrons are transferred from water molecules to FEP, forming a negatively charged $(FEP)e^-$ surface. The released O_2 subsequently scavenges these electrons, regenerating the neutral FEP surface and completing the CE cycle. Density functional theory (DFT) calculations revealed that the transient high-pressure environment created by bubble collapse lowers the energy barriers for electron transfer by ~18% for water/FEP and ~23% for $(FEP)e^-/O_2$, thereby markedly accelerating interfacial charge-exchange. Unlike conventional sonochemistry, which typically employs high-frequency ultrasound (up to ~1 MHz) to optimize cavitation-driven bond-breaking, CE-Chemistry generally operates at much lower frequencies (20–100 kHz). In this regime, ultrasound exerts predominantly mechanical effects, enhancing mass transport, activating interfaces and inducing frequent contact-separation cycles that facilitate interfacial electron transfer.[113] Furthermore, the influence of ultrasonic parameters on CE-Chemistry was systematically investigated using FEP powder for MO degradation across a wide range of frequencies (20–89 kHz), powers (120–600 W), and temperatures (10–50 °C).[114] At 20 °C, the strongest enhancement was achieved at 40 kHz and 600 W, identifying these as the optimal ultrasonic conditions for FEP-mediated CE-Chemistry. Temperature-dependent studies further showed that the reaction efficiency peaked between 20–30 °C, beyond which the degradation performance declined. Importantly, comprehensive post-reaction analyses, including scanning electron microscopy (SEM), energy-dispersive X-ray spectroscopy (EDX), X-ray photoelectron spectroscopy, Raman spectroscopy, and Fourier-transform infrared (FTIR) spectroscopy, consistently demonstrated that triboelectric materials (powders, films, beads, tubes, and stir bars) retain their structural and chemical integrity after repeated mechanical operation. This robustness highlights their durability and supports the feasibility of their sustainable, long-term application in triboelectric catalytic systems.

2.2.3. Theoretical and computational insights into CE-Chemistry. Existing studies provide important mechanistic

support for the physical plausibility of contact-induced chemical reactivity. Early simulations in CE-Chemistry relied on DFT to calculate the energy barriers between a solid (*e.g.*, PTFE) and a liquid molecule to prove that electron transfer is thermodynamically possible. In a seminal study, Wang *et al.* performed DFT calculations to estimate the electron-transfer barriers at solid dielectric–water interfaces and between charged solid dielectrics and O_2, proposing that cavitation-induced high pressures reduce these barriers and thereby facilitate the formation of ROS (Fig. 5a).[10] These calculations support the idea that mechanical stimulation under CE can modulate the interfacial electron-transfer energetics. However, they are necessarily based on simplified, largely static interface models and therefore do not capture the stochastic, non-equilibrium nature of real CE processes. Subsequent computational studies introduced electronic-structure descriptors to rationalize the material dependence in CE-Chemistry. By evaluating the frontier molecular orbitals and vertical electron-attachment energies of representative polymers, DFT calculations suggested that materials with stronger electron-accepting characteristics tend to accumulate higher negative charge upon contact, correlating with their enhanced CE-Chemical activity.[115] More recent simulations have extended CE-Chemistry to reaction-specific scenarios, such as CO_2 reduction. In these studies, DFT calculations were employed to evaluate the adsorption energetics, density-of-states modulation, and interfacial charge-redistribution at catalytic sites, for example metal single atoms supported on charged polymer substrates (Fig. 5b).[100] Furthermore, Jin *et al.* demonstrated that CE generates strong interfacial electric fields capable of lowering the activation barriers for bond cleavage, such as C–F scission in the degradation of per- and poly-fluoroalkyl substances

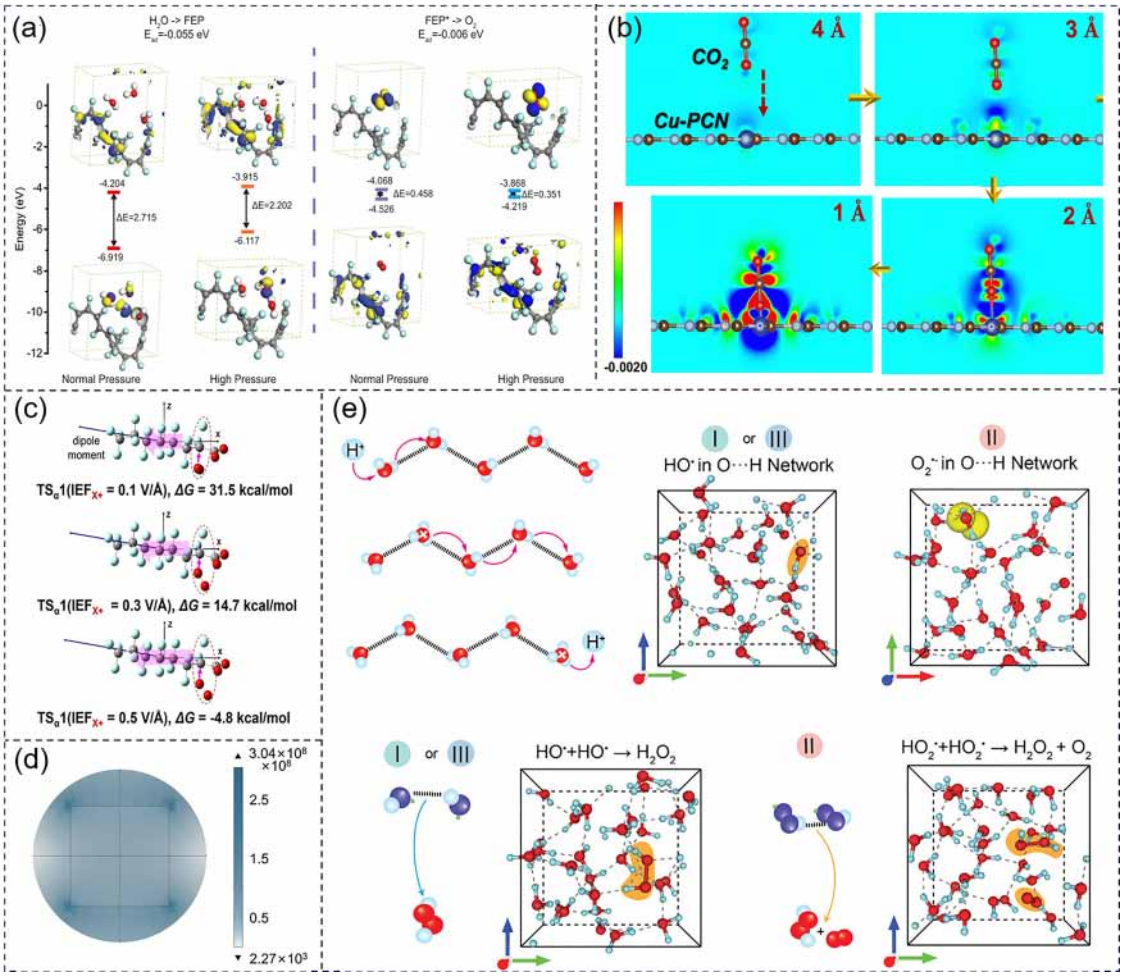

Fig. 5 Theoretical and computational insights into CE-Chemistry. (a) DFT calculations of the values of the LUMO and HOMO levels for water-FEP and O_2-FEP in various conditions. Reproduced from ref. 10 with permission from Springer Nature, copyright 2022. (b) Charge distribution near the single Cu atom-anchored polymeric carbon nitride (Cu-PCN) surface during contact. Reproduced from ref. 100 with permission from Springer Nature, copyright 2024. (c) Transient state (TS) and reaction energy barriers (ΔG) for the $\cdot O_2^-$ nucleophilic reaction under an interfacial electric field of 0.3 V Å^{-1}. Reproduced from ref. 116 with permission from John Wiley and Sons, copyright 2024. (d) COMSOL simulation results of the PTFE electrostatic field. Reproduced from ref. 118 with permission from Elsevier, copyright 2025. (e) Illustration of proton hopping by the Grotthuss mechanism in water hydrogen bond network and results of the AIMD simulation of the hydrogen bond network under 30% densification of the aqueous solution for various steps. Reproduced from ref. 119 with permission from John Wiley and Sons, copyright 2023.

(PFAS) (Fig. 5c).[116] Fan *et al.* proved that the surface charge on FEP significantly lowers the energy barrier for the rate-determining step (activation of the C–H bond) through DFT calculation, making the reaction thermodynamically feasible at room temperature.[117] Finite element simulations validated the physical mechanism by quantifying the interfacial electric field. Studies confirmed that the electric field strength surrounding PTFE reached a maximum of 3.04×10^8 V m^{-1} (Fig. 5d), thereby facilitating the generation of ROS.[118]

Addressing the limitations of static models, *ab initio* molecular dynamics (AIMD) can simulate the dynamic environment of a liquid–solid interface. For example, it shows how water molecules crash into the catalyst surface and split into radicals ($\cdot$OH and $\cdot O_2^-$) under the influence of an electric field. Specifically, it visualized that $\cdot$OH and $\cdot O_2^-$ do not diffuse randomly; instead, they migrate *via* proton hopping (Grotthuss mechanism) through the water hydrogen-bond network, explaining the unexpectedly high reaction rates[119] (Fig. 5e). Moreover, both DFT and AIMD have been used to demonstrate that the mechanical impact of ultrasound cavitation physically breaks atomic bonds on the solid dielectric surface, creating dynamic defects that act as transient catalytic active sites.[120] Current theoretical investigations provide robust mechanistic validation for CE-Chemistry, effectively transitioning this field from empirical phenomenology to a predictive chemical science. The integration of these computational tools underscores a critical synergy, where static DFT confirms thermodynamic feasibility through CE-induced barrier lowering, while AIMD elucidates the kinetic origins of reactivity, identifying mechanisms such as proton-coupled transport (Grotthuss mechanism) and dynamic defect formation. Nevertheless, existing simulations often rely on idealized interface models that may oversimplify complex stochastic environments. Moving forward, the theoretical frontier of CE-Chemistry lies in the development of integrated multiscale modeling frameworks. By bridging atomic-scale charge-transfer events with macroscopic interfacial electric field distributions, future research can guide the rational design of CE surfaces for maximizing the efficiency of CE-Chemistry.

2.2.4. Interfacial reaction pathways driven by CE-Chemistry. A prototypical CE-Chemistry redox cycle has been proposed,[121] where reactant A transfers electrons to the surface of a solid dielectric (C) upon contact, generating oxidized A (A_{oxd}) and a triboelectrically charged surface state (C*). After desorption of A_{oxd}, the charge-storing surface state C* donates electrons to a second reactant B, reducing it to B_{red} while regenerating the neutral surface C, thereby completing the cycle. This model underscores one fundamental role of the solid dielectric: to serve as a temporary reservoir for transferred charge, which in turn drives redox reactions in the adjacent liquid environment. Furthermore, growing evidence indicates that CE-Chemistry is substantially more complex than this idealized two-step electron-shuttling picture, involving strongly coupled pathways of interfacial electron transfer, radical generation, and proton-mediated processes. These contributions operate synergistically, and their mutual interactions collectively govern both the thermodynamic driving forces and the reaction kinetics. In the following section, several representative mechanistic cases are highlighted to illustrate how CE modulates reaction pathways. Together, these examples demonstrate the unique capability of CE-Chemistry as a promising platform for green synthesis and environmental remediation.

2.2.4.1. Reactions enabled by interfacial electron transfer. Extensive evidence shows that contact–separation between a solid dielectric and a liquid generates and stores excess electrons on the dielectric surface.[122] Materials with stronger electron-withdrawing character accumulate higher charge densities, establishing localized interfacial electric fields that lower activation barriers and directly promote reductive transformations. Direct spectroscopic evidence for CE-mediated electron transfer was provided by Wang *et al.* using the paramagnetic probe TEMPO.[123] Because TEMPO undergoes a one-electron/one-proton reduction to TEMPOH, attenuation of its EPR signal reports on electron availability. The reduction efficiencies of different triboelectric materials (FEP > PTFE > PP > high-density polyethylene (HDPE) > control) mirrored their solid dielectric–water CE outputs, revealing a quantitative correlation between CE charge generation and catalytic electron-transfer capability. These stored electrons reduced a broad range of metal ions, including $[AuCl_4]^-$, Pd^{2+}, $[PtCl_4]^{2-}$, Ag^+, Rh^{3+} and Ir^{3+}, in aqueous solution (Fig. 6a), and the reduction trend for $[AuCl_4]^-$ matched that observed for TEMPO. Building on this framework, Zhang *et al.* showed that triboelectrically accumulated electrons on negatively charged PTFE can directly reduce $[AuCl_4]^-$, enabling the CE-driven synthesis of gold nanoparticles (AuNPs) in the absence of conventional reducing agents.[124] Their work established that nanoparticle nucleation and growth proceed purely *via* CE-mediated interfacial electron transfer. Xing and *et al.* further demonstrated that charged fluorocarbon polymers (FCPs) operate as efficient charge reservoirs that reduce Fe^{3+} under the guidance of interfacial electric fields (Fig. 6b).[125] Electrons accumulated at the FEP interface drive rapid Fe^{3+}/Fe^{2+} cycling, while the concomitant generation of H_2O_2 and Fe^{2+} initiates a robust Fenton process, achieving a sulfadiazine degradation rate of 0.125 min^{-1}. Electron-transfer-mediated Fe cycling was likewise observed in a CE-Chemistry system based on iron-loaded mesoporous carbon (Fe/OMC).[126] Mei *et al.* extended CE-driven reduction to the fabrication of silver-decorated PTFE composites (PTFE-Ag).[127] Under ultrasonication, PTFE generated triboelectrically accumulated electrons that accelerated Ag^+ reduction and locally enriched Ag^+ at the interface. The resulting Ag nanoparticles, uniformly deposited and exhibiting clear lattice fringes, confirmed a direct interfacial electron-transfer pathway (Fig. 6c). In our recent work, CE between glass or PTFE beads and water likewise enabled Ag^+ reduction (Fig. 6d).[128] These observations support a synergistic mechanism in CE-Chemistry comprising: (i) direct interfacial electron transfer from tribocharged dielectric surfaces and (ii) indirect reduction *via* $\cdot O_2^-$ generated during O_2 activation. Collectively, these studies show that triboelectrically accumulated electrons can efficiently reduce diverse metal-ion redox couples, including Fe^{3+}/Fe^{2+}, Ag^+/Ag and Au^{3+}/Au, firmly

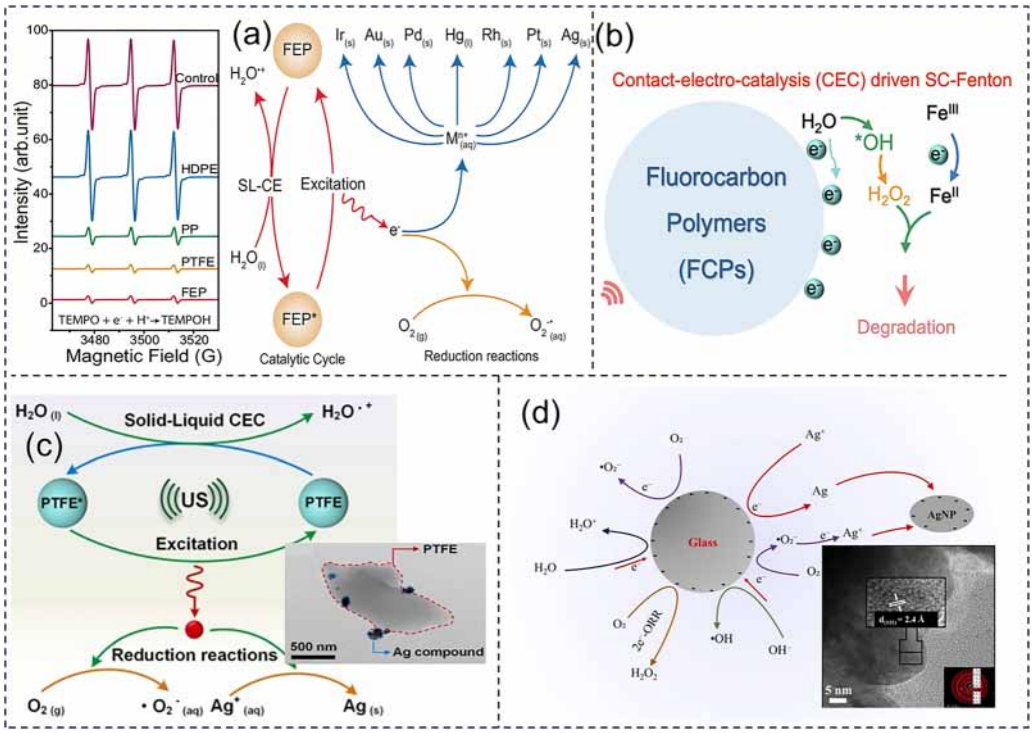

Fig. 6 CE-Chemistry enabled by interfacial electron-transfer. (a) EPR detection of TEMPO in CE-Chemistry with various triboelectric materials and schematic of the reduction of various metal ions (M^{n+}) in the aqueous solution by ultrasonically driven CEC in the presence of FEP. Reproduced from ref. 123 with permission from Springer Nature, copyright 2024. (b) Fe^{3+}-driven self-cycling Fenton process *via* CEC for water purification. Reproduced from ref. 125 with permission from Springer Nature, copyright 2025. (c) Formation of plasmonic silver particles *via* CEC mediated by acoustic–solid interactions. Reproduced from ref. 127 with permission from Elsevier, copyright 2025. (d) Synergistic effects in triboelectric charge-driven redox reactions. Reproduced from ref. 128 with permission from Elsevier, copyright 2025.

establishing interfacial electron transfer as a defining and generalizable mechanistic pathway in CE-Chemistry.

2.2.4.2. Reactions initiated by radical intermediates. Radical pathways represent one of the most prevalent mechanistic routes in CE-Chemistry. In particular, ·OH, $\cdot O_2^-$ and singlet oxygen are frequently generated at solid dielectric–liquid interfaces during CE and subsequently drive pollutant degradation, oxidative transformations and polymerization reactions. Therefore, detecting and characterizing these short-lived intermediates is essential for elucidating interfacial electron-transfer processes in chemically complex CE systems.[129,130] Jiang *et al.* showed that water droplets produce ·OH upon contacting PTFE, silicone rubber or nylon-6, with the radical yields following the electron-withdrawing ability of the materials (PTFE > silicone rubber > nylon-6).[110] The ·OH signal increased markedly from pH 7 to 13, consistent with its origin in the CE-induced oxidation of OH^- (Fig. 7a). By contrast, $\cdot O_2^-$ was not detected under static conditions but appeared upon ultrasonication, which provides the activation energy required for electron transfer to dissolved O_2 and thereby enables efficient tetracycline degradation. However, it is worth noting that conducting the experiments under N_2 to suppress O_2 may inherently limit $\cdot O_2^-$ formation in the absence of ultrasonication. Wang *et al.* further verified CE-driven ROS production using EPR, detecting both ·OH and $\cdot O_2^-$ (Fig. 7b).[10] Their results indicate that single-electron oxidation of interfacial water at the FEP surface produces $^\bullet$OH, whereas electrons accumulated on the tribo-charged FEP reduce dissolved O_2 to $\cdot O_2^-$. The latter is protonated to $HO_2\cdot$ and can be converted to ·OH through secondary reactions, together establishing a robust oxidative environment for organic pollutant removal. Jiang *et al.* also observed the characteristic 1 : 2 : 2 : 1 ·OH quartet on SiO_2 microspheres, accompanied by oxidative and reductive fluorescence signals attributed to the formation of $^\bullet$OH and H$^\bullet$, respectively (Fig. 7c).[131] In addition, Yuan *et al.* demonstrated that CE markedly enhances peroxymonosulfate (PMS) activation.[132] In the US/FEP/PMS system, EPR spectra revealed both DMPO-·OH (quartet) and DMPO-$SO_4\cdot^-$ (sextet) adducts, which were absent in US/PMS alone, showing that the CE-generated electrons on FEP activate PMS to form highly reactive sulfate radicals (Fig. 7d). CE-induced radical chemistry is not restricted to aqueous media; in a recent study, a non-aqueous FEP-DMSO system produced both $\cdot O_2^-$ and methyl radicals ($CH_3^\bullet$), enabling efficient phenol degradation *via* coupled radical pathways (Fig. 7e).[17] Collectively, these studies establish that CE can generate a diverse suite of radical intermediates across aqueous and non-aqueous environments. By modulating interfacial charge-transfer, solvent identity and mechanical input, CE-Chemistry offers a tunable platform for directing radical formation and controlling interfacial reaction pathways.

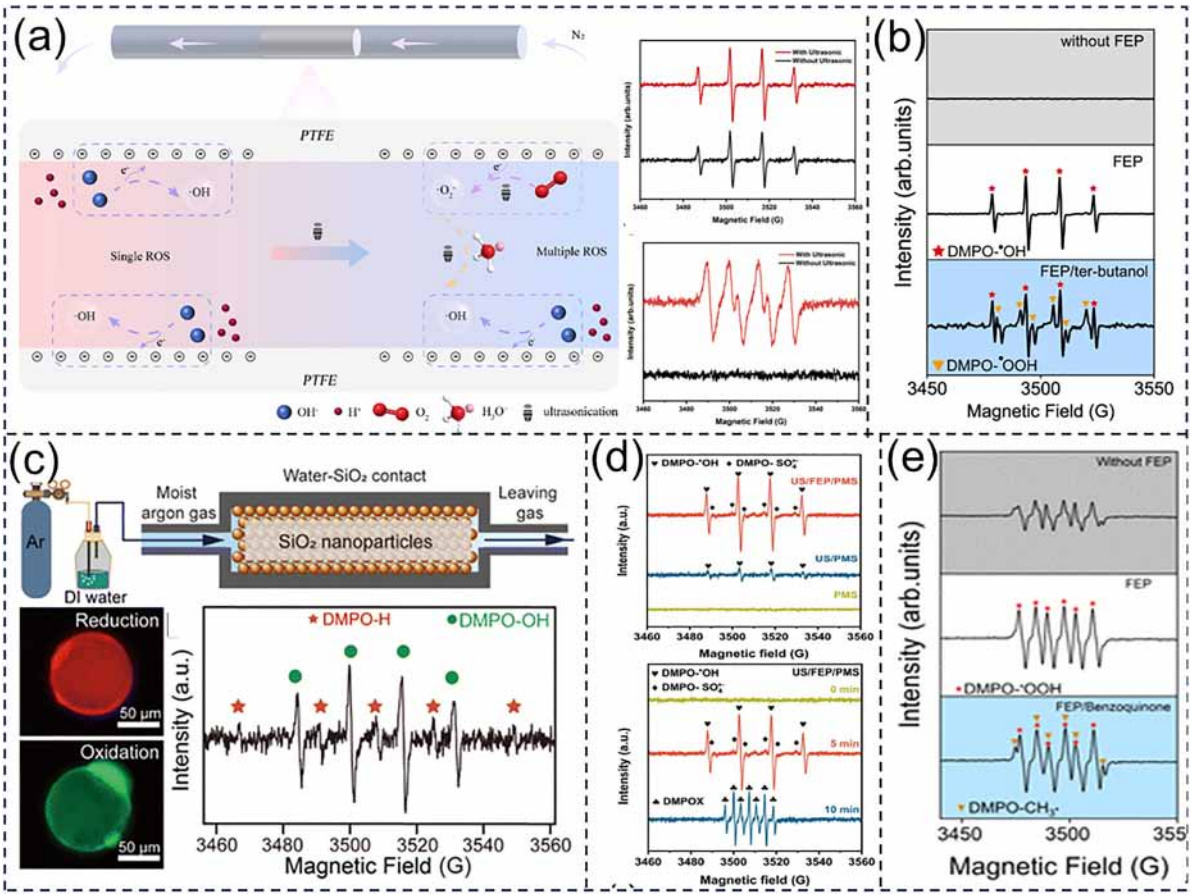

Fig. 7 CE-Chemistry initiated by radical intermediates. (a) Process of free radical generation during CE at a solid dielectric–liquid interface. Reproduced from ref. 110 with permission from Elsevier, copyright 2023. (b) EPR spectrum measurement detecting radicals produced from FEP-water CE. Reproduced from ref. 10 with permission from Springer Nature, copyright 2022. (c) Fluorescence microscopy image of reductive/oxidative species and the corresponding ESR signals from SiO_2 microspheres after contact with water-carrying argon gas. Reproduced from ref. 131 with permission from the Royal Society of Chemistry, copyright 2024. (d) EPR evidence of PMS activation triggered by CEC. Reproduced from ref. 132 with permission from Springer Nature, copyright 2025. (e) Formation of $^{\bullet}O_2^-$ and $CH_3^{\bullet}$ radicals in the PTFE-DMSO CE-Chemistry system. Reproduced from ref. 17 with permission from the American Chemical Society, copyright 2024.

2.2.4.3. Proton-mediated reactivity. Tang *et al.* showed that MO degradation in an FEP-water CE-Chemistry system is maximized at neutral pH.[133] Similarly, Liu *et al.* reported that a low-cost EPDM catalyst activates PMS to remove >90% of tetracycline within 30 min, again with an optimal performance near pH 7.[134] Consistent with these trends, PTFE-driven H_2 evolution also peaks at pH 7 and decreases under both acidic and alkaline conditions.[135] Yuan *et al.* further observed that pentachlorophenol (PCP) degradation is strongly suppressed at pH 3–5 relative to neutral conditions (Fig. 8a).[136] Under acidic conditions, PCP exists predominantly as neutral C_6Cl_5OH, which is less susceptible to oxidative radical attack, whereas at neutral to alkaline pH it is converted to the more soluble and reactive pentachlorophenolate ($C_6Cl_5O^-$). However, at high pH, excess OH^- scavenges ·OH, thereby diminishing the overall degradation efficiency. Across these systems, the pH dependence of CE-Chemistry activity is governed primarily by ion-induced screening, which inhibits interfacial electron transfer. Wang *et al.* demonstrated that increasing the ionic strength *via* the addition of electrolytes, such as H^+ or OH^-, screens local interfacial electric fields and suppresses electron transfer between water and PTFE.[81] Because CE charge generation relies on this interfacial electron transfer, excessive ion concentrations inevitably reduce triboelectric charge production. Protons are particularly effective suppressors, where in acidic media, fast-diffusing H^+ transiently adsorbs onto PTFE during contact–separation, competing with electron transfer through physical and electrostatic interactions.[137]

Even when CE-Chemistry is initiated at neutral pH, progressive solution acidification is commonly observed as reactions proceed. As shown in Fig. 8b, DI water rapidly acidifies under ultrasonication in the presence of FEP.[18] Gao *et al.* similarly reported a pH decrease from 5.6 to 3.6 over 4 h in a PTFE-water system.[138] This acidification arises because electron loss from water to FEP generates transient water radical cations, which undergo proton transfer to form H_3O^+ and ·OH.[139–143] On the one hand, the accumulated H^+ establishes an interfacial EDL that suppresses further electron transfer. In line with this picture, Zhan *et al.* showed that ion-rich droplets generate substantially less triboelectric charge than pure water, owing

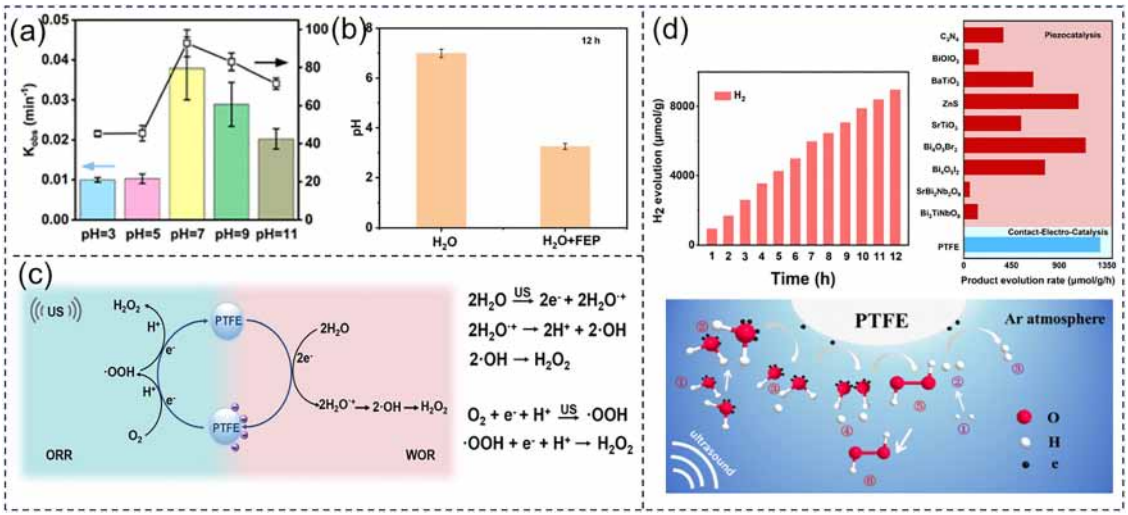

Fig. 8 Proton-mediated reactivity in CE-Chemistry. (a) Reaction rate constants (bars, left axis) and PCP degradation (black line, right axis) under CE-Chemical conditions at different pH levels. Reproduced from ref. 136 with permission from the American Chemical Society, copyright 2024. (b) Comparison of the pH of DI water with and without FEP powder after 12-h ultrasonication. Reproduced from ref. 18 with permission from the American Chemical Society, copyright 2025. (c) Proposed CEC reaction mechanism for H_2O_2 generation. Reproduced from ref. 11 with permission from John Wiley and Sons, copyright 2023. (d) H_2 evolution *via* electron capture by interfacial protons to form $^{\bullet}H$, with durability assessment and comparison to piezocatalytic H_2 production. Reproduced from ref. 135 with permission from the Royal Society of Chemistry, copyright 2025.

to interfacial electric field screening.[144] On the other hand, H^+ can actively participate in CE-Chemistry processes. Fan *et al.* recently clarified the coupled proton–electron dynamics underlying CE-driven H_2O_2 formation, which proceeds *via* two coordinated half-reactions: water oxidation and oxygen reduction (Fig. 8c).[11] In the oxidative branch, CE-induced interfacial charge-transfer produces water radical cations that rapidly yield H_3O^+ and ·OH, followed by ·OH recombination to form H_2O_2. Notably, this direct $^{\bullet}OH$ formation typically requires extremely high anodic potentials, which are inaccessible in conventional electrocatalysis.[145,146] In parallel, dissolved O_2 in collapsing cavitation bubbles captures interfacial electrons to form $\cdot O_2^-$, which is protonated to ·OOH and further reduced to H_2O_2. Because the initial electron-transfer step ($O_2 + e^- \rightarrow \cdot O_2^-$) demands a more negative potential than the classical $2e^-$ ORR route, synchronized proton and electron availability at the CE interface is essential.

The importance of this coupled dynamics extends beyond H_2O_2 generation. Zare *et al.* recently reported a CE-driven ammonia-synthesis pathway in which protons from water reduce N_2 adsorbed on triboelectrically charged PTFE surfaces, without any applied voltage or irradiation.[12] More broadly, recent studies show that proton-involved pathways can couple constructively with triboelectric electron transfer to drive CE-Chemistry. Huang *et al.* demonstrated direct H_2 production from pure water under CE-Chemistry conditions, even in Ar-saturated environments, where protons serve as the sole electron acceptor (Fig. 8d).[135] Prolonged mechanical activation of PTFE increased the H_2 yields to 1286.6 μmol g^{-1} h^{-1}. In this system, negatively charged PTFE particles accumulate electrons during repeated contact-separation events and reduce interfacial protons to $^{\bullet}H$ intermediates, which subsequently recombine to form H_2 ($2H^+ + 2e^- \rightarrow H_2$). Ultrasonic agitation further accelerates this process by generating abundant solid–liquid interfaces and transient microcavitation sites. The linear increase in H_2 production over 12 h (up to 8952.7 μmol g^{-1}, with a mechanical-to-hydrogen efficiency of 0.17%) highlights both the robustness of the CE interface and its potential for sustainable hydrogen generation. Proton reduction is accompanied by partial water oxidation, yielding H_2O_2 as a parallel pathway.

2.3. Role of interfacial electric fields in CE-Chemistry

It is well established that interfacial electric fields exert a profound influence on electron dynamics. This principle is clearly illustrated by the design of a polymer/metal Janus composite catalyst that regulates the rates of the water oxidation reaction (WOR) and ORR *via* CE-Chemistry.[147] Theoretical simulations were performed to evaluate the CE-derived electric field and its impact on the work function of the metallic side. The charge density on the FEP surface after CE with water was first estimated from experimental measurements, and then COMSOL Multiphysics was used to simulate the strength of the CE-induced electric field at different separation distances between the metal and polymer (Fig. 9a). The electric field strength decays sharply as the separation increases from 100 nm to 1 μm, indicating an intense electric field ($\sim 10^8$ V m^{-1}) in the immediate vicinity of the FEP film. The calculated Fermi level of Cu under interfacial electric fields of varying magnitudes and directions further shows that the Cu Fermi level decreases from 4.325 to 2.88 eV as the electric field strength increases from 0 to 10^8 V m^{-1} in the presence of a negatively charged FEP film, implying that less energy is required for Cu to donate electrons to the solution. The ability of a triboelectrically charged FEP layer to tune the metal work function and

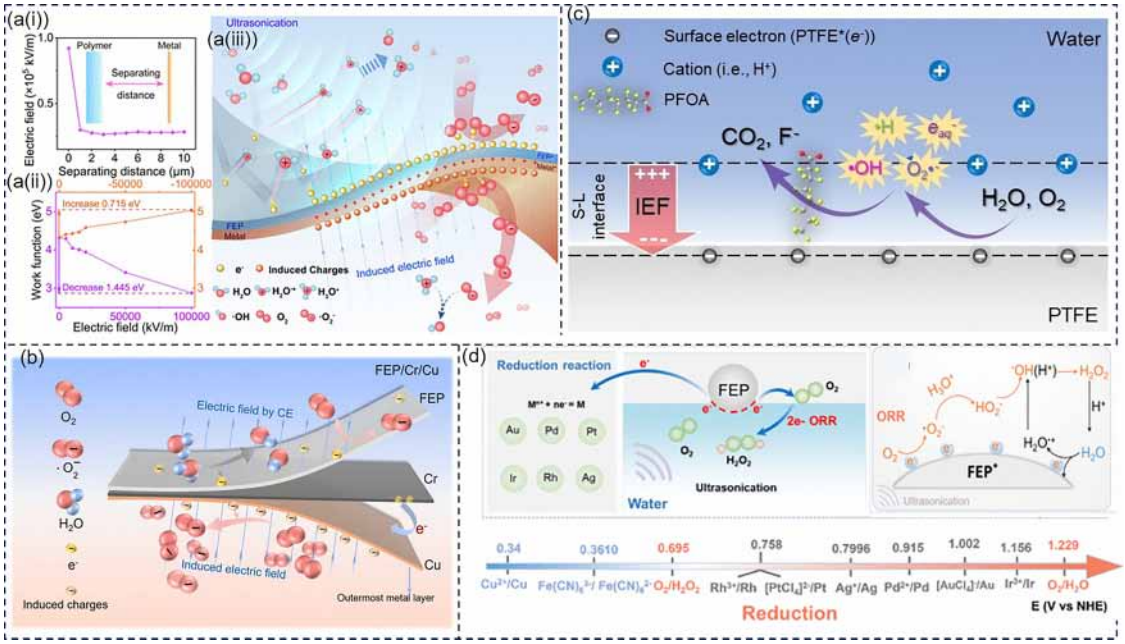

Fig. 9 Role of interfacial electric fields in CE-Chemistry. (a(i)) Simulated CE-derived interfacial electric fields, (a(ii)) calculated work-function evolution of Cu under varying electric field strengths and (a(iii)) proposed operating mechanism for enhancing the CEC efficiency in the presence of polymer/metal Janus catalysts. Reproduced from ref. 147 with permission from the American Chemical Society, copyright 2024. (b) Modular CE-Chemistry enabled by dielectrics with metal coatings that allow work-function tuning. Reproduced from ref. 148 with permission from Elsevier, copyright 2025. (c) Interfacial electric fields driving C–F bond cleavage in perfluoroalkyl substances under CEC conditions. Reproduced from ref. 116 with permission from John Wiley and Sons, copyright 2024. (d) Janus chemical pathways in CE-Chemistry elucidated through the ORR. Reproduced from ref. 18 with permission from the American Chemical Society, copyright 2025.

enhance its reducing power provides compelling evidence that a strong interfacial electric field is established during solid dielectric–liquid CE, functioning analogously to an effective electrode–electrolyte potential difference. Building on this concept, our recent work employed dielectric polymer/multilayer-metal architectures to optimize interfacial electron transfer and enhance CE-driven reactivity.[148] As shown in Fig. 9b, triboelectric charge on the FEP surface generates a strong interfacial electric field that electrostatically polarizes the underlying metal, driving electron accumulation at its outer surface. These induced electrons, being less tightly bound than those on FEP, more readily participate in oxygen reduction. The high electric field intensity simultaneously lowers the metal work function and polarizes interfacial water, thereby accelerating ·OH formation. In multilayer metal stacks, electronegativity differences provide an additional lever for regulating electron flow. In FEP/Cr/Cu, electrons migrate from Cr to Cu, increasing the surface charge on Cu, lowering its work function and enhancing $\cdot O_2^-$ generation *via* ORR. Reversing the order (FEP/Cu/Cr) withdraws electrons from Cr, reducing its surface charge, increasing its work function and suppressing ORR. Together, electrostatic induction from the CE-generated interfacial electric field and electron redistribution within the metal layers furnish a synergistic strategy for tuning ORR activity and improving the CE-Chemistry efficiency.

Jin *et al.* further demonstrated that in a US/PTFE system the high surface voltage generated by CE produces a strong interfacial electric field at the PTFE–water interface, which markedly influences the reactivity of perfluorooctanoic acid (PFOA). As shown in Fig. 9c, CE renders the PTFE surface negatively charged, generating surface voltages on the order of tens to hundreds of volts.[116] On the aqueous side, the compensating cations form a Stern layer, and together with the intrinsic hydrophobic gap between PTFE and water, spanning a few to several tens of Å,[81] define a nanometric region in which an intense interfacial electric field of $\sim 10^9$–10^{10} V m^{-1} develops. This electric field strongly activates PFAS molecules and lowers the barrier for $\cdot O_2^-$-driven nucleophilic attack. Beyond this, our previous work linked CE-Chemical reactivity directly to the standard electrode potentials (SEPs) of the ORR-relevant redox couples. We found that the redox selectivity in CE-Chemistry is governed by a threshold SEP (Fig. 9d), where metal ions with SEPs above the 2e$^-$ ORR potential (E° = 0.695 V *vs.* SHE) undergo reduction (for example $[AuCl_4]^-$, Pd^{2+}, $[PtCl_4]^{2-}$, Ag^+, Rh^{3+} and Ir^{3+}), whereas species with lower SEPs, such as ferrocyanide, preferentially undergo oxidation.[18] This clear SEP-dependent selectivity indicates that CE establishes a localized interfacial potential drop, and thus a hidden electric field capable of supplying the free-energy difference required to surmount these redox thresholds.

Solid dielectrics with hydrophobic characteristics have attracted considerable attention as efficient platforms for exploiting solid–liquid CE, as these surfaces promote effective contact-separation dynamics between liquid and solid interfaces.[149] In particular, fluorinated solid dielectrics, which are intrinsically hydrophobic, exhibit strong electron-withdrawing capability and

are frequently associated with enhanced CE performances.[140] From a mechanistic perspective, Lin *et al.* reported that ion transfer dominates solid–liquid CE on hydrophilic surfaces, whereas electron transfer becomes the primary charge-transfer pathway on hydrophobic surfaces.[83] Complementarily, Wang *et al.* proposed that electron transfer is driven predominantly by the work-function difference between liquid and superhydrophobic surfaces.[150] These observations collectively suggest that constructing interfaces between water and hydrophobic solid dielectrics provides a favorable environment for electron-transfer-dominated CE, thereby facilitating CE-Chemistry. Importantly, the chemical characteristics associated with water-hydrophobic interfaces are not restricted to solid dielectrics but can also arise in gas–liquid and liquid–liquid systems involving hydrophobic phases (*e.g.*, oils). These related interfacial configurations have attracted increasing attention and are briefly discussed in the following sections for broader perspectives.

3. Hidden electric fields at gas–liquid interfaces

Liu *et al.* attributed the rapid oxidation of SO_2 in microdroplets to the unique electrostatic environment of the air–water interface rather than bulk-phase chemistry.[151] Raman mapping combined with MD simulations revealed pronounced surface enrichment of NO_3^- and SO_4^{2-}, forming an interfacial ion layer that generates a built-in electric field approaching $\sim 10^{10}$ V m^{-1}, as quantified by SERS-Stark spectroscopy (Fig. 10a). Sulfate formation rates increase with both the degree of ion segregation and the magnitude of the interfacial electric field, confirming that the kinetics are interface-controlled. Previous studies have shown that interfacial electric fields on the order of $\sim 10^7$–10^8 V m^{-1} can polarize bond dipoles and weaken O–H bonds.[43] DFT calculations further indicate that partial solvation and strong interfacial electrostatics stabilize charge-separated transition states, establishing the interfacial electric field as a primary driver of accelerated SO_2 oxidation in microdroplets. Complementary insight comes from Jackson *et al.*, who proposed an alternative origin for strong microdroplet interfacial fields based on the alignment of surface-active organic molecules at gas–liquid interfaces.[152] Using the voltage-sensitive fluorophore 4-Di-1-ASP, they showed that only interfacial electric fields applied perpendicular to the interface induce emission shifts, with the peak positions scaling linearly with electric field strength ($R^2 > 0.99$) (Fig. 10b). Confocal fluorescence imaging revealed an interfacial emission red-shift of 18 nm, and combined solvatochromic and DFT analyses indicated local interfacial electric fields of (0.46–1.3) $\times$ 10^9 V m^{-1}. Remarkably, this enhanced electric field extends $\sim$1 μm into the droplet and is largely insensitive to salt concentrations up to 2 M, suggesting that classical charge-separation models (Debye screening) alone cannot account for the large electric field. Instead, dipole-aligned organic layers at

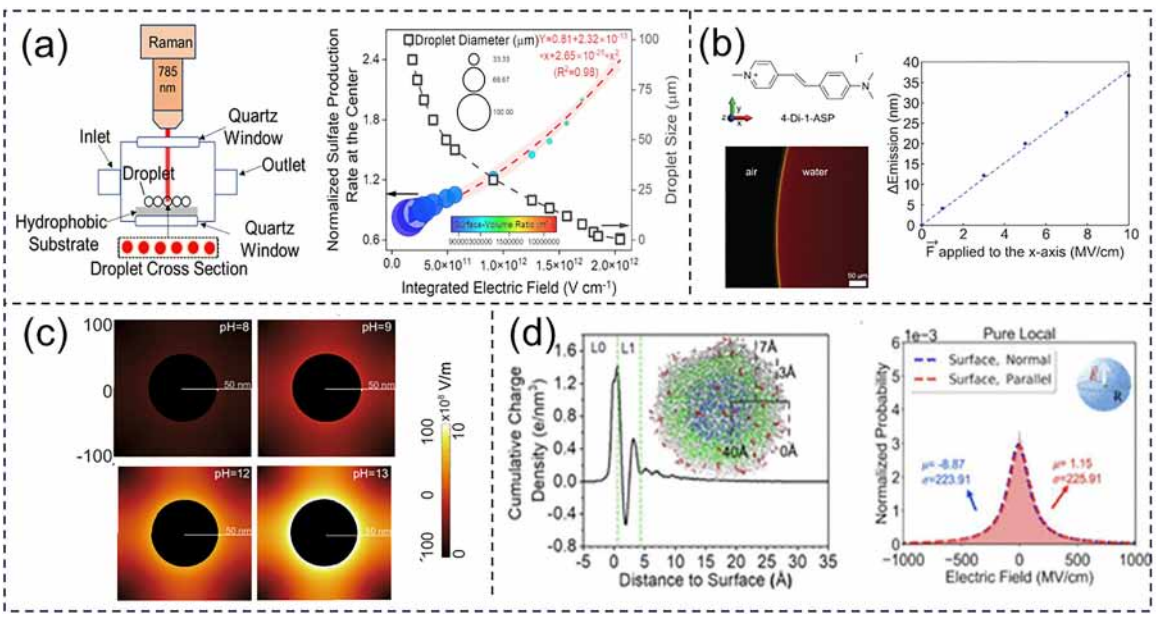

Fig. 10 Hidden electric fields at gas–liquid interfaces. (a) SERS measurement and Au-NaSCN probe assembly illustrating sulfate production as a function of the integrated interfacial electric field (10 vol%) and its dependence on the droplet size. Reproduced from ref. 151 with permission from Elsevier, copyright 2023. (b) Spectral confocal microscopy image of a water-droplet cross-section containing 0.1 mM 4-Di-1-ASP (2.9 nm spectral resolution), and corresponding emission-maximum shifts relative to the zero electric field value as a function of electric field applied along the chromophore *x*-axis. Reproduced from ref. 152 with permission from the American Chemical Society, copyright 2025. (c) COMSOL-simulated electric field distribution at the gas–liquid interface of the bubbles. Reproduced from ref. 153 with permission from Springer Nature, copyright 2025. (d) Cumulative charge density at the air–water interface of nanodroplets simulated using the reactive ReaxFF/C-GeM force field, showing nanoscale fluctuations, and the corresponding Lorentzian distribution of interfacial electric fields derived from the same simulations. Reproduced from ref. 43 with permission from Springer Nature, copyright 2022.

the air–water boundary provide a robust additional source of strong interfacial electric fields. *In situ* chemiluminescence imaging, spectroscopy and multiscale simulations show that OH^- enrichment at microbubble surfaces, together with strong interfacial electric fields, enables catalyst-free ·OH formation.[153] Simulations indicate that the interfacial electric field reaches 1.02×10^9 V m^{-1} at pH 13 and increases with alkalinity (Fig. 10c).[153] Under UV irradiation at pH 12, the local OH^- concentration near the bubble surface becomes ~69-fold higher than in the bulk solution, placing OH^- in a highly activated state where electron loss readily generates •OH. These findings highlight how interfacial enrichment and electric field amplification act synergistically to promote radical formation at gas–liquid boundaries. Head-Gordon *et al.* systematically quantified the charge density, surface potential and local interfacial electric fields in water nanodroplets, focusing on those experienced by interfacial O–H vibrational modes (Fig. 10d).[43] They reported an average interfacial electric field of $\sim 10^9$ V m^{-1}, consistent with SREF measurements. Although the mean electric field lies below the threshold for direct bond dissociation, the inherently flexible air–water interface produces a broad Lorentzian distribution of instantaneous electric field intensities. Transient high electric field events within this distribution can transiently reach values capable of modulating chemical reactivity. Related studies further underscore the critical role of interfacial electric field fluctuations in governing microdroplet chemistry.[46,47]

The charging of separated droplets also underpins a range of natural electrostatic phenomena. As early as 1752, Franklin demonstrated that conductive rods could attract lightning to charge a Leyden jar, and in 1892 Lenard showed that splashing and bubbling induce charge separation at water surfaces.[154,155] Modern calculations indicate that microdroplet separation can generate interfacial electric fields approaching $\sim 10^9$ V m^{-1},[156] which are strong enough to oxidize OH^- to ·OH and form H_2O_2. The charge carried by sprayed droplets has been visualized by high-speed imaging and quantified using Kelvin probe force microscopy (KPFM).[157] Localized interfacial electric fields of similar magnitude arise when smaller negatively charged droplets transfer charge to larger positively charged ones. Depending on their size and formation conditions, water microdroplets can carry either a positive or negative net charge,[158–162] and open-air mass spectrometry detects ionic species such as N_2^+, O_2^+, NO^+ and NO_2^+. Meng *et al.* further showed that sprayed water droplets emit luminescence in the absence of an applied voltage,[163] consistent with ''microlightning'' capable of exciting, ionizing or dissociating nearby molecules. Thus, microdroplets function simultaneously as high-activity microreactors and rapid transport carriers. Multiple mechanisms have been proposed to account for their unusual reactivity, including confinement-enhanced encounters, partial solvation, preferential reactant orientation, curvature effects and pronounced pH deviations at the air–water interface.[34,164–167] However, increasing attention has converged on strong interfacial electric fields at the gas–liquid boundary as a central contributor to microdroplet chemistry.[168,169] Min *et al.* further proposed that these intrinsic interfacial electric fields fundamentally reshape the chemical kinetics and thermodynamics at air–water boundaries, offering a promising strategy for engineering interfacial reactivity and aqueous-phase synthesis.[169]

At present, the physical origins of electric fields at gas–liquid interfaces remain incompletely understood. In this review, we propose that CE constitutes one of the mechanistic origins of interfacial electric fields across diverse chemical interfaces. Experimental evidence for CE-mediated charging at gas–liquid interfaces has been obtained using low-power, portable acoustic levitation platforms, which enable liquid droplets to be suspended in controlled gaseous environments.[170] Under acoustic excitation, levitated droplets undergo rapid rotational motion, giving rise to sustained tribological interactions between the liquid surface and the surrounding gas. The net charge accumulated on the droplets increases progressively with levitation time and eventually approaches a saturation limit upon prolonged suspension. This behavior is consistent with a non-equilibrium charging process at gas–liquid interfaces, in which surface charge gradually accumulates before reaching a quasi-equilibrium state, with potential implications for interfacial chemical reactivity. Further evidence supporting the potential role of CE in microdroplet charging has been provided by Wang *et al.*, who proposed that CE-induced charging of water microdroplets contributes to the development of strong interfacial electric fields.[156] By analyzing the diameter distributions of oppositely charged droplets, they observed that positively charged droplets are generally larger than negatively charged ones. Based on this asymmetry, the electric field established between oppositely charged droplets during separation was estimated to reach approximately 10^9 V m^{-1}. These field strengths have been proposed to be sufficient to promote OH^- oxidation to ·OH, offering experimental support for the possible involvement of CE-related interfacial electric fields in the spontaneous formation of H_2O_2 in microdroplet systems. In addition, the formation of microdroplets commonly involves gas–liquid jetting through confined channels composed of solid dielectric materials, under which conditions repeated gas–liquid–solid interactions are unavoidable. Comparable flow architectures have been extensively investigated in TENG systems, where the combined effects of CE and electrostatic induction have been demonstrated to generate electrical potentials on the order of kilovolts.[171] These observations further suggest that CE is likely involved in charge generation during dynamic gas–liquid transport, although it might not be the sole contributing mechanism. Beyond mechanistic investigations, gas–liquid atomization-based TENGs have also been employed for the degradation of organic dyes, illustrating concrete chemical applications of two-phase CE processes.[172]

4. Hidden electric fields at liquid–liquid interfaces

Min's group has provided key insights into the molecular and electrostatic landscapes at liquid–liquid interfaces, substantially advancing the mechanistic understanding of microdroplet and

emulsion chemistry. In 2020, they employed stimulated Raman-excited fluorescence (SREF) spectroscopy to directly quantify the local interfacial electric fields at water–oil interfaces (Fig. 11a). Using a nitrile-bearing chromophore as a vibrational Stark reporter, they revealed exceptionally strong interfacial electric fields ($\sim 10^9$ V m^{-1}) oriented normal to the droplet surface.[44] Interfacial electric fields of this magnitude are sufficient to polarize reactants and lower activation barriers, providing a physical basis for the long-observed rate acceleration of chemical reactions in microdroplets. This work established that, even in the absence of an external bias, spontaneous charge separation at curved liquid interfaces can generate electrostatic environments comparable to those in electrochemical cells. More recently, Min *et al.* probed the water structure within oil-in-water emulsion droplets using interface-selective Raman spectroscopy combined with spectral decomposition and theoretical modelling (Fig. 11b).[173] They showed that the interfacial water within oil droplets differs markedly from bulk water, where hydrogen bonding is weakened, tetrahedral order is reduced and a substantial population of "free O–H" groups emerges, with its stretching modes red-shifted by ~ 95 cm^{-1} relative to planar oil–water interfaces. In light of the well-established electrostatic zeta potentials of oil droplets,[174] they proposed the presence of a strong electric field ($\sim(5\text{–}9) \times 10^9$ V m^{-1}) emanating from the oil phase. Together, these results highlight structural disorder and enhanced interfacial electric fields as defining features of mesoscale oil–water interfaces, which may contribute directly to the accelerated reactivity observed at hydrophobic–water boundaries.[34] Beyond emulsions, Dai *et al.* reported that phase separation itself can generate interfacial electric fields at condensate–solution interfaces.[45] They observed an interfacial electric field of $\sim 5 \times 10^6$ V m^{-1} arising from ion and molecular density gradients across the liquid–liquid boundary (Fig. 11c), enabling spontaneous redox chemistry both *in vitro* and in living cells. Subsequent work by the same group showed that even in the absence of net charge, hydrophobicity asymmetry across condensates can create interphase electric potentials corresponding to interfacial electric fields on the order of 10^8 V m^{-1}.[175] Taken as a whole, these studies establish electric field generation at liquid–liquid boundaries as a generic interfacial phenomenon, not restricted to ionic segregation, with broad implications for biological, chemical and soft-matter systems.

Similarly, CE at liquid–liquid interfaces should not be overlooked in the context of this review. By exploiting gravitational effects and molecular mass differences, liquid droplets in this system were able to move freely without external mechanical forcing. As droplets continuously fell and contacted one another, the amount of transferred charge on the droplet surface gradually attenuated and ultimately reached a saturation state. Complementary studies further demonstrated that CE at liquid–liquid interfaces can involve both electron and ion transfer processes.[176] Together, these observations indicate that CE-mediated charge-transfer at liquid–liquid interfaces represents an important pathway for the establishment of interfacial electric fields. Beyond charge accumulation, liquid–liquid CE has also been directly linked to chemical reactivity. At liquid–liquid boundaries, Jiang *et al.* showed that ultrasonication-induced perfluorocarbon-water CE drives electron transfer from water into the perfluorocarbon phase, leading to the generation of ·OH and $\cdot O_2^-$ radicals.[177,178] Notably, ·OH formation could be further enhanced by the presence of H_2O_2 even in the absence of ultrasound.[178] These findings demonstrate that liquid–liquid interfaces can function as radical-generating platforms *via* CE, highlighting their potential utility in chemical and therapeutic applications, including tumor treatment.

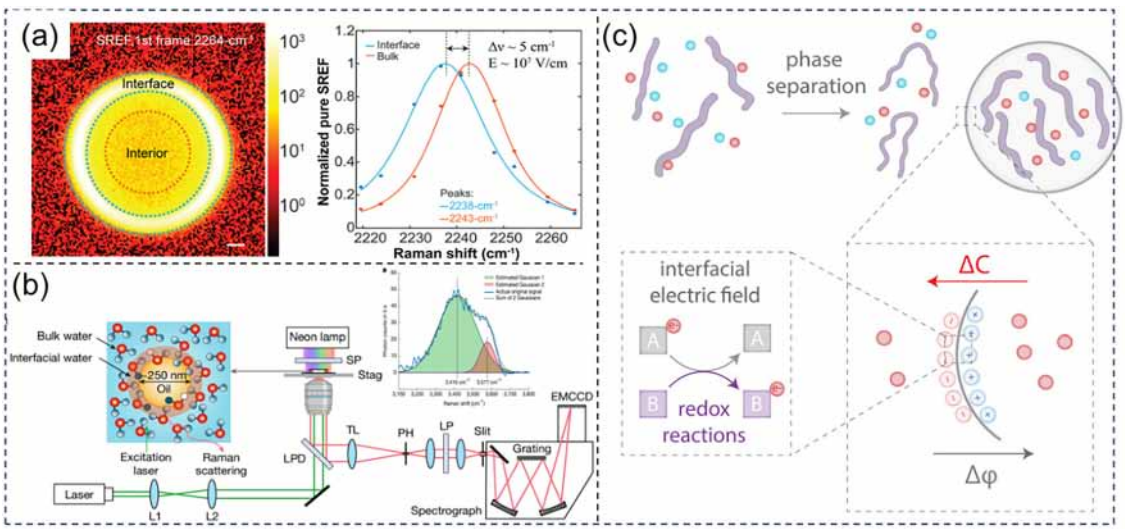

Fig. 11 Hidden electric fields at liquid–liquid interfaces. (a) First frame of hyperspectral SREF imaging and solute-correlated Rh800 nitrile-mode spectra of a water microdroplet in hexadecane. Reproduced from ref. 44 with permission from the American Chemical Society, copyright 2020. (b) Schematic of a custom-built confocal micro-Raman system and oil-perturbed water spectra of oil droplets. Reproduced from ref. 173 with permission from Springer Nature, copyright 2025. (c) Surface electrostatics of condensates inducing EDL formation for driving redox reactions. Reproduced from ref. 45 with permission from Elsevier, copyright 2023.

5. Perspective and outlook

"God made the bulk, the surface was invented by the devil," remarked Wolfgang Pauli.[179] Yet it is precisely at surfaces and interfaces that nearly all interactions with the external world occur, from tactile perception to catalytic turnover. The recognition of interfacial electric fields has become a focal point of growing interest, although recent debates continue regarding the potential contribution of isobaric interferences or evaporation-induced concentration gradients.[180–182] A wide body of experimental observations and theoretical analyses now indicates that electric fields are intrinsically generated at interfaces. Across a wide range of water–hydrophobic interfaces, measured interfacial electric fields consistently converge near $\sim 10^9$ V m^{-1}.[169] These interfacial electric fields are largely equilibrium (or quasi-equilibrium) in nature and arise from cooperative contributions including hydroxide enrichment, oriented water dipoles, dielectric discontinuities and interfacial charge-transfer,[173,183,184] and have been quantified by vibrational Stark spectroscopy, electrochromic probes, Raman-MCR analysis and electrokinetic measurements.[44,152,185] Despite notable advances, key challenges remain, particularly in understanding how distinct interfacial environments give rise to different interfacial electric fields through variations in molecular organization, charge-transfer pathways, and dynamics. Importantly, Hao *et al.* demonstrated that the mean interfacial electric field alone is insufficient to account for certain chemical reactivities. Instead, rare but intense local field fluctuations, occupying the high-field tail of a Lorentzian distribution, can substantially lower the activation barriers for specific reactions.[43] These extreme field events occur on timescales comparable to molecular vibrations and solvent relaxation, indicating that field-reactant coupling at interfaces is inherently dynamic rather than static. A similar picture emerges from 3D atomic force microscopy and theory, where CE-induced surface charging was shown to markedly reorganize the interfacial hydration layer and modulate the water structure at the atomic scale.[186] *In situ* measurements reveal hydration-layer oscillations comparable to those observed in electrochemical systems, implying that CE-driven interfacial electric fields can initiate redox processes mechanistically analogous to faradaic reactions, yet without applied bias and driven solely by CE-induced electron transfer and radical chemistry. From this perspective, these observations indicate that solid–liquid, gas–liquid, and liquid–liquid interfaces, where charging processes are intrinsically dynamic, are likely to share a common reactivity origin arising from transient, high-intensity interfacial electric field fluctuations.

As illustrated in Fig. 12, this review identifies interfacial electric fields as a common underlying factor, offering a unifying conceptual framework for rationalizing a broad class of anomalous interfacial chemical phenomena that are not readily captured by bulk-phase descriptors alone. The growing recognition that interfacial electric fields can be both strong and highly structured compels a reassessment of many analytical and technological frameworks that implicitly assume electric field-free interfaces. Techniques such as interfacial spectroscopy, flow-based separations and kinetic profiling may all be influenced, or even dominated, by CE-active conditions that impose hidden potential drops. In this context, regulation of interfacial electric fields emerges as a potentially powerful route toward green chemistry, providing a fundamentally different strategy for driving and tuning chemical transformations through interfacial electric fields, rather than relying on conventional catalytic or electrochemical paradigms. For CE-Chemistry, the interfacial electric fields that arise at multiphase CE interfaces are poised to reshape how high-efficiency reaction systems are designed and how multiphase interfacial reactivity is understood. By deliberately engineering these interfacial electric fields, through device architecture, material selection and controlled contact dynamics, it should become possible to steer electron transfer, radical generation and redox pathways with unprecedented precision, enabling greener and more energy-efficient chemistries.

By harnessing interfacial electric fields as a pivotal and tunable driving forces for chemical reactivity, CE circumvents the need for noble metals, facilitating self-powered catalytic pathways for nitrogen fixation, urea synthesis, and carbon sequestration. Utilizing inert and recyclable dielectric materials, this approach establishes a highly sustainable paradigm that transcends traditional energy and environmental boundaries, unlocking multifaceted utilities across an expansive landscape of emerging chemical technologies. Within CE-Chemistry, the electric field generated during CE is now emerging as a decisive parameter governing reaction pathways, efficiencies

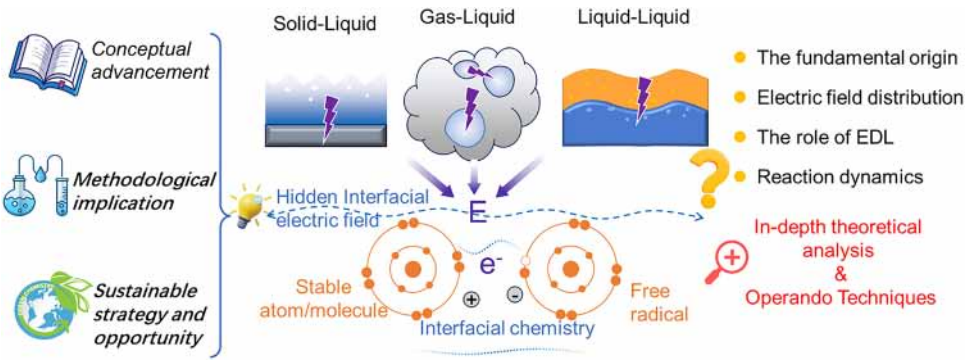

Fig. 12 Challenges and opportunities of interfacial electric fields in chemistry.

and selectivity. Material properties such as electronegativity, bandgap, surface functionality and dielectric constant dictate the extent of interfacial electron transfer, rendering fluorinated polymers particularly effective at establishing large potential drops across nanoconfined interfaces.[139] Because these interfacial electric fields originate from mechanically driven charge transfer, their magnitude is inherently sensitive to the strength, frequency and mode of mechanical stimulation. In ultrasound-induced CEC, Tang *et al.* estimated the transferred charge per contact-separation event and, by combining this with contact frequency, calculated the total flux of activation electrons under ultrasonication.[114] Their analysis indicates that the CE-Chemistry efficiency is essentially dictated by the number of activated electrons generated during CE; these electrons seed subsequent ROS-generation pathways and thereby initiate CEC. This observation motivates deeper questions including how can these ''activation electrons'' be regulated and how are nearby ions perturbed by the evolving local electric field to participate in downstream CE-Chemistry? Once triboelectric charge is established on a solid dielectric surface, the adjacent liquid phase critically governs the subsequent evolution of the interfacial electric field and its effectiveness in driving chemical activation. Ionic strength controls the rate and extent of EDL reconstruction, partially screening the electric field and suppressing additional electron transfer when the EDL becomes overly compact.[81] Dynamic pH variations, arising from proton consumption or generation and associated radical chemistry, feed back into interfacial ion adsorption–desorption equilibria, thereby reshaping the local electric field gradients. Solvent molecular structure dictates which radical species are favored under strong interfacial electric field conditions, where water predominantly yields ·OH and $\cdot O_2^-$, whereas aprotic solvents such as DMSO favor C–S bond polarization and methyl radical ($^{\bullet}CH_3$) formation.[17] Dissolved gases add yet another layer of control. O_2, N_2 or CO_2 can serve as competitive electron or radical scavengers, redirecting reaction pathways toward $\cdot O_2^-$ formation or CO_2 reduction depending on the electric field strength, solubility and molecular accessibility.[187–190] Taken together, these factors emphasize that the CE-Chemistry reactivity is not simply a function of the presence of triboelectric charge, but emerges from dynamic coupling among mechanical input, material properties, solvent architecture and ionic environment, which collectively determine how the hidden electric field is generated, distributed and ultimately transduced into chemical transformation. From an application perspective, interfacial electric fields generated through CE-Chemistry enable low-cost reaction systems with minimal reliance on an external bias and, importantly, without the need for conventional counter electrodes, thereby avoiding the parasitic side reactions commonly encountered in traditional electrochemical setups. This feature renders CE-Chemistry particularly attractive for green and potentially recyclable CO_2 transformation. However, significant challenges remain, including limited efficiency gains for multi-electron CO_2 reduction, insufficient control over product selectivity, and the integration of CO_2 capture with interfacial field-driven activation. Looking forward, CE-Chemistry might not be regarded as a standalone alternative to conventional catalysis, but rather as a synergistic strategy that can be integrated with traditional electrochemical methods to locally amplify interfacial electric fields. These hybrid approaches may offer a viable pathway toward efficient, low-energy, and scalable electrochemical technologies for greenhouse gas mitigation.

Taken together, CE-driven reactions typically proceed more rapidly during the initial stages of CE,[114] mirroring the temporal profile of charge transfer in these systems.[144] This correspondence indicates that interfacial reactions are preferentially promoted under non-equilibrium, CE-generated electric fields, which exhibit pronounced temporal fluctuations and spatial heterogeneity.[186] At these early stages, electron transfer dominates and leads to charge accumulation on the solid surface, which in turn modulates concurrent ion migration within the liquid phase.[83] The resulting synergistic interplay between transient CE-generated fields and evolving ionic redistribution dynamically perturbs the interfacial electric field, thereby initiating and influencing interfacial chemical reactions. As the CE process continues, ion migration progressively promotes the formation and stabilization of the EDL,[73,191] corresponding to an equilibrium screening regime. Once a compact and fully developed EDL is established, strong ionic screening significantly suppresses further interfacial electron transfer,[144] thereby inhibiting subsequent CE-driven chemical reactions. This framework mechanistically explains why CE performance and CE-Chemistry efficiency might be diminished in high-ionic-strength environments, where rapid EDL formation could suppress effective interfacial charge-transfer. Conversely, in organic solvents such as DMSO, where free ions are limited yet CE activity persists, the formation of a stabilized EDL might be impeded.[17,192] Under these conditions, non-equilibrium CE-generated fields persist for longer durations, leading to more efficient phenol degradation and methanol oxidation compared to aqueous systems.[17,18] It should be emphasized that this framework is presented as a working hypothesis, grounded in current experimental observations and theoretical insights. Further comprehensive experimental and theoretical investigations are required to quantitatively delineate the contributions of non-equilibrium CE-generated fields and equilibrium EDL effects, as well as their dynamic interplay during interfacial chemical reactions.

1. Theoretical models linking triboelectric charge to interfacial electric fields.

A key challenge in CE-Chemistry lies in developing theoretical frameworks that translate CE-generated triboelectric charge into spatially and temporally resolved interfacial electric fields relevant to chemical reactivity. Such models must connect molecular-scale interfacial processes with experimentally accessible quantities, including surface charge density and surface potential. Achieving this requires tight integration of theory and experiment, combining electrostatic and molecular simulations with direct benchmarks from TENG-based charge measurements and KPFM surface potential mapping. To capture realistic CE conditions, models should be implemented within dynamic simulation frameworks that account for contact-

separation cycles and the evolution of the EDL. Physics-informed machine learning approaches may further accelerate model development, provided that physical constraints are rigorously enforced.

2. Resolving the spatial distribution of interfacial electric fields at Ångström-nanometer scales.

Determining how interfacial electric fields are spatially distributed and localized across molecular length scales is essential for connecting electric field strength to specific reaction coordinates and active sites. Vibrational Stark effect spectroscopy, using calibrated IR or Raman probes, provides a quantitative measurement of local electric field strength. Complementarily, sum-frequency generation (SFG) spectroscopy offers insight into field-induced molecular orientation and interfacial ordering. Three-dimensional atomic force microscopy (3D-AFM) permits direct visualization of hydration-layer structures and electrostatic landscapes with sub-nanometer resolution, while scanning tunneling microscopy (STM) can probe atomic-scale potential variations in conductive systems.

3. Understanding EDL screening and electric field reshaping.

A central mechanistic challenge is to quantify how EDL formation screens, localizes, or amplifies interfacial electric fields under both equilibrium and non-equilibrium conditions. Techniques such as zeta potential measurements and electrochemical impedance spectroscopy (EIS) provide insight into EDL formation and dynamics, while surface-sensitive methods including X-ray photoelectron spectroscopy (XPS) and neutron reflectometry resolve the ion and solvent layering perpendicular to solid–liquid interfaces. Systematic variation of ionic strength and counter-ion identity, combined with reaction kinetics, allows causal assessment of EDL effects on interfacial reactivity.

4. Coupling dynamic field fluctuations to reaction coordinates.

Beyond static field descriptions, a critical challenge is to elucidate how rapid, transient interfacial electric field fluctuations couple to electron-transfer events, bond activation, and radical formation. Time-resolved spectroscopic techniques are essential for probing such dynamics. Scanning ion conductance microscopy (SICM), with its high sensitivity to local ionic currents, provides a direct means to visualize ion migration and EDL perturbations under CE conditions, enabling the discrimination of CE-generated non-equilibrium fields from equilibrium electrostatic contributions.

Conflicts of interest

There are no conflicts to declare.

Data availability

No primary research results, software or codes have been included, and no new data were generated or analyzed as part of this review.

Acknowledgements

We thank Richard N. Zare for his valuable comments on the original manuscript. This work was supported by the National Natural Science Foundation (grant number 22479016).

References

1 M. Ciobanu, J. P. Wilburn, M. L. Krim and D. E. Cliffel, 1 - Fundamentals, in *Handbook of Electrochemistry*, ed. C. G. Zoski, Elsevier, Amsterdam, 2007, pp. 3–29.
2 S. Srinivasan, Evolution of electrochemistry, *In Fuel Cells: From Fundamentals to Applications*, Springer, 2006, pp. 3–25.
3 P. S. Adarakatti, Fundamentals of electrochemistry, *In Agricultural Electrochemistry*, ACS Publications, 2025, pp. 17–46.
4 T. S. Wesley, Y. Román-Leshkov and Y. Surendranath, Spontaneous Electric Fields Play a Key Role in Thermochemical Catalysis at Metal-Liquid Interfaces, *ACS Cent. Sci.*, 2021, **7**(6), 1045–1055.
5 A. Warshel, P. K. Sharma, M. Kato, Y. Xiang, H. Liu and M. H. M. Olsson, Electrostatic Basis for Enzyme Catalysis, *Chem. Rev.*, 2006, **106**(8), 3210–3235.
6 S. D. Fried, S. Bagchi and S. G. Boxer, Extreme electric fields power catalysis in the active site of ketosteroid isomerase, *Science*, 2014, **346**(6216), 1510–1514.
7 Y. Chai, W. Dai, G. Wu, N. Guan and L. Li, Confinement in a Zeolite and Zeolite Catalysis, *Acc. Chem. Res.*, 2021, **54**(13), 2894–2904.
8 C. Liu and A. J. Bard, Electrostatic electrochemistry at insulators, *Nat. Mater.*, 2008, **7**(6), 505–509.
9 J. Zhang, S. Lin and Z. L. Wang, Electrostatic Charges Regulate Chemiluminescence by Electron Transfer at the Liquid–Solid Interface, *J. Phys. Chem. B*, 2022, **126**(14), 2754–2760.
10 Z. Wang, A. Berbille, Y. Feng, S. Li, L. Zhu, W. Tang and Z. L. Wang, Contact-electro-catalysis for the degradation of organic pollutants using pristine dielectric powders, *Nat. Commun.*, 2022, **13**(1), 130.
11 J. Zhao, X. Zhang, J. Xu, W. Tang, Z. Lin Wang and F. Ru Fan, Contact-electro-catalysis for Direct Synthesis of H_2O_2 under Ambient Conditions, *Angew. Chem., Int. Ed.*, 2023, **62**(21), e202300604.
12 J. Li, Y. Xia, X. Song, B. Chen and R. N. Zare, Continuous ammonia synthesis from water and nitrogen via contact electrification, *Proc. Natl. Acad. Sci. U. S. A.*, 2024, **121**(4), e2318408121.
13 H. Li, A. Berbille, X. Zhao, Z. Wang, W. Tang and Z. L. Wang, A contact-electro-catalytic cathode recycling method for spent lithium-ion batteries, *Nat. Energy*, 2023, **8**(10), 1137–1144.
14 S. Li, Z. Zhang, P. Peng, X. Li, Z. L. Wang and D. Wei, A green approach to induce and steer chemical reactions using inert solid dielectrics, *Nano Energy*, 2024, **122**, 109286.

15 C. Xu, S. Li, Y. Zhang, Z. Wang, Z. L. Wang and D. Wei, Contact-electro-chemistry induced by flow electrification in dielectric tubes, *Nano Energy*, 2025, **134**, 110526.
16 C. Xu, S. Li, Z. Yang, M. Willatzen, Z. Lin Wang and D. Wei, Contact-electro-luminescence triggered by triboelectric charge, *Chem. Eng. J.*, 2024, **501**, 157754.
17 J. Liu, Z. Yang, S. Li, Y. Du, Z. Zhang, J. Shao, M. Willatzen, Z. L. Wang and D. Wei, Nonaqueous Contact-Electro-Chemistry via Triboelectric Charge, *J. Am. Chem. Soc.*, 2024, **146**(46), 31574–31584.
18 T. Gan, Z. Yang, S. Li, H. Qian, Z. Li, J. Liu, P. Peng, J. Bai, H. Liu, Z. Wang and D. Wei, Unveiling Janus Chemical Processes in Contact-Electro-Chemistry through Oxygen Reduction Reactions, *J. Am. Chem. Soc.*, 2025, **147**(29), 25407–25416.
19 D. Xing, X. Yuan, C. Liang, T. Jin, S. Zhang and X. Zhang, Spontaneous oxidation of I^- in water microdroplets and its atmospheric implications, *Chem. Commun.*, 2022, **58**(89), 12447–12450.
20 D. Zhang, X. Yuan, C. Gong and X. Zhang, High Electric Field on Water Microdroplets Catalyzes Spontaneous and Ultrafast Oxidative C–H/N–H Cross-Coupling, *J. Am. Chem. Soc.*, 2022, **144**(35), 16184–16190.
21 C. Gong, D. Li, X. Li, D. Zhang, D. Xing, L. Zhao, X. Yuan and X. Zhang, Spontaneous Reduction-Induced Degradation of Viologen Compounds in Water Microdroplets and Its Inhibition by Host–Guest Complexation, *J. Am. Chem. Soc.*, 2022, **144**(8), 3510–3516.
22 L. Qiu and R. G. Cooks, Simultaneous and Spontaneous Oxidation and Reduction in Microdroplets by the Water Radical Cation/Anion Pair, *Angew. Chem., Int. Ed.*, 2022, **61**(41), e202210765.
23 X. Song, Y. Meng and R. N. Zare, Spraying Water Microdroplets Containing 1,2,3-Triazole Converts Carbon Dioxide into Formic Acid, *J. Am. Chem. Soc.*, 2022, **144**(37), 16744–16748.
24 H. Chen, R. Wang, J. Xu, X. Yuan, D. Zhang, Z. Zhu, M. Marshall, K. Bowen and X. Zhang, Spontaneous Reduction by One Electron on Water Microdroplets Facilitates Direct Carboxylation with CO_2, *J. Am. Chem. Soc.*, 2023, **145**(4), 2647–2652.
25 X. Yuan, D. Zhang, C. Liang and X. Zhang, Spontaneous Reduction of Transition Metal Ions by One Electron in Water Microdroplets and the Atmospheric Implications, *J. Am. Chem. Soc.*, 2023, **145**(5), 2800–2805.
26 S. Jin, H. Chen, X. Yuan, D. Xing, R. Wang, L. Zhao, D. Zhang, C. Gong, C. Zhu, X. Gao, Y. Chen and X. Zhang, The Spontaneous Electron-Mediated Redox Processes on Sprayed Water Microdroplets, *JACS Au*, 2023, **3**(6), 1563–1571.
27 Q. He, N. Zhang, Y. Qiao, C. Li and J. Zhang, Vapor generation of mercury and methylmercury in aqueous microdroplets produced by pneumatic nebulization, *J. Anal. At. Spectrom.*, 2022, **37**(9), 1894–1901.
28 M. A. Mohajer, P. Basuri, A. Evdokimov, G. David, D. Zindel, E. Miliordos and R. Signorell, Spontaneous formation of urea from carbon dioxide and ammonia in aqueous droplets, *Science*, 2025, **388**(6754), 1426–1430.
29 B. R. Layman, D. M. Carrel and J. E. Dick, Multiphase Electrochemiluminescence of Microdroplets and Radical Salts, *Acc. Chem. Res.*, 2025, **58**(12), 1856–1866.
30 R. A. LaCour, J. P. Heindel, R. Zhao and T. Head-Gordon, The Role of Interfaces and Charge for Chemical Reactivity in Microdroplets, *J. Am. Chem. Soc.*, 2025, **147**(8), 6299–6317.
31 M. Girod, E. Moyano, D. I. Campbell and R. G. Cooks, Accelerated bimolecular reactions in microdroplets studied by desorption electrospray ionization mass spectrometry, *Chem. Sci.*, 2011, **2**(3), 501–510.
32 X. Yan, Emerging microdroplet chemistry for synthesis and analysis, *Int. J. Mass Spectrom.*, 2021, **468**, 116639.
33 J. K. Lee, S. Kim, H. G. Nam and R. N. Zare, Microdroplet fusion mass spectrometry for fast reaction kinetics, *Proc. Natl. Acad. Sci. U. S. A.*, 2015, **112**(13), 3898–3903.
34 Z. Wei, Y. Li, R. G. Cooks and X. Yan, Accelerated Reaction Kinetics in Microdroplets: Overview and Recent Developments, *Annu. Rev. Phys. Chem.*, 2020, **71**, 31–51.
35 Z. Zhou, X. Yan, Y.-H. Lai and R. N. Zare, Fluorescence Polarization Anisotropy in Microdroplets, *J. Phys. Chem. Lett.*, 2018, **9**(11), 2928–2932.
36 A. Malevanets and S. Consta, Variation of droplet acidity during evaporation, *J. Chem. Phys.*, 2013, **138**, 18.
37 J. D. Rindelaub, R. L. Craig, L. Nandy, A. L. Bondy, C. S. Dutcher, P. B. Shepson and A. P. Ault, Direct measurement of pH in individual particles via Raman microspectroscopy and variation in acidity with relative humidity, *J. Phys. Chem. A*, 2016, **120**(6), 911–917.
38 T. Müller, A. Badu-Tawiah and R. G. Cooks, Accelerated Carbon–Carbon Bond-Forming Reactions in Preparative Electrospray, *Angew. Chem., Int. Ed.*, 2012, **51**(47), 11832–11835.
39 A. K. Badu-Tawiah, D. I. Campbell and R. G. Cooks, Accelerated C–N Bond Formation in Dropcast Thin Films on Ambient Surfaces, *J. Am. Soc. Mass Spectrom.*, 2012, **23**(9), 1461–1468.
40 K. R. Wilson and A. M. Prophet, Chemical Kinetics in Microdroplets, *Annu. Rev. Phys. Chem.*, 2024, **75**, 185–208.
41 F. Galembeck, L. P. Santos, T. A. L. Burgo and A. Galembeck, The emerging chemistry of self-electrified water interfaces, *Chem. Soc. Rev.*, 2024, **53**(5), 2578–2602.
42 K. Y. Chan, C. Zhuang, V. G. Vuong, N. Qian, X. Gao and W. Min, Electric fields at hydrophobic water interfaces: spectroscopic evidence, physical origin, and implications on reactivity, *Chem. Soc. Rev.*, 2026, **55**(1), 336–357.
43 H. Hao, I. Leven and T. Head-Gordon, Can electric fields drive chemistry for an aqueous microdroplet?, *Nat. Commun.*, 2022, **13**(1), 280.
44 H. Xiong, J. K. Lee, R. N. Zare and W. Min, Strong Electric Field Observed at the Interface of Aqueous Microdroplets, *J. Phys. Chem. Lett.*, 2020, **11**(17), 7423–7428.
45 Y. Dai, C. F. Chamberlayne, M. S. Messina, C. J. Chang, R. N. Zare, L. You and A. Chilkoti, Interface of biomolecular condensates modulates redox reactions, *Chem*, 2023, **9**(6), 1594–1609.

46 M. T. C. Martins-Costa and M. F. Ruiz-López, Electrostatics and Chemical Reactivity at the Air–Water Interface, *J. Am. Chem. Soc.*, 2023, **145**(2), 1400–1406.
47 M. T. C. Martins-Costa and M. F. Ruiz-López, Probing solvation electrostatics at the air–water interface, *Theor. Chem. Acc.*, 2023, **142**(3), 29.
48 J. A. Nauman, D. Suvlu and A. P. Willard, Electric Fields at Solid-Liquid Interfaces: Insights from Molecular Dynamics Simulation, *Annu. Rev. Phys. Chem.*, 2025, **76**, 181–202.
49 G. Gonella, E. H. G. Backus, Y. Nagata, D. J. Bonthuis, P. Loche, A. Schlaich, R. R. Netz, A. Kühnle, I. T. McCrum, M. T. M. Koper, M. Wolf, B. Winter, G. Meijer, R. K. Campen and M. Bonn, Water at charged interfaces, *Nat. Rev. Chem.*, 2021, **5**(7), 466–485.
50 B. Yang, K. Liu, H. Li, C. Liu, J. Fu, H. Li, J. E. Huang, P. Ou, T. Alkayyali and C. Cai, Accelerating CO2 electroreduction to multicarbon products via synergistic electric–thermal field on copper nanoneedles, *J. Am. Chem. Soc.*, 2022, **144**(7), 3039–3049.
51 S. Li, J. Zhang, Y. Li, P. Fan and M. Wu, Revisiting N, S co-doped carbon materials with boosted electrochemical performance in sodium-ion capacitors: The manipulation of internal electric field, *Nano Res. Energy*, 2024, **3**, 1.
52 Y. Shen, P. Fu, J. Liu, K. Sun, H. Wen, P. Liu, H. Lv, T. Gu, X. Yang and L. Chen, Highly stable Zn anodes realized by 3D zincophilic and hydrophobic interphase buffer layer, *Nano Res. Energy*, 2024, **3**(3), e9120115.
53 Q. Chen; J. Huang; D. Chu; L. Cao; X. Li; Y. Zhao; Y. Liu; J. Dong and L. Feng, *In Accelerated Photogenerated Charge Separation Driven Synergistically by the Interfacial Electric Field and Work Function in Z-Scheme Zn-Ni2P/G-C3N4 for Efficient Photocatalytic Hydrogen Evolution, Exploration*, Wiley Online Library, 2025, p. 20240189.
54 C. Cai, K. Liu, L. Zhang, F. Li, Y. Tan, P. Li, Y. Wang, M. Wang, Z. Feng and D. Motta Meira, Atomically local electric field induced interface water reorientation for alkaline hydrogen evolution reaction, *Angew. Chem., Int. Ed.*, 2023, **62**(26), e202300873.
55 L. Du, H. Xiong, H. Lu, L. M. Yang, R. Z. Liao, B. Y. Xia and B. You, *Electroshock synthesis of a bifunctional nonprecious multi-element alloy for alkaline hydrogen oxidation and evolution, Exploration*, Wiley Online Library, 2022, p. 20220024.
56 Y. Zhou, Y. Liang, J. Fu, K. Liu, Q. Chen, X. Wang, H. Li, L. Zhu, J. Hu and H. Pan, Vertical Cu nanoneedle arrays enhance the local electric field promoting C2 hydrocarbons in the CO2 electroreduction, *Nano Lett.*, 2022, **22**(5), 1963–1970.
57 H. Li, H. Zhou, Y. Zhou, J. Hu, M. Miyauchi, J. Fu and M. Liu, Electric-field promoted C–C coupling over Cu nanoneedles for CO2 electroreduction to C2 products, *Chin. J. Catal.*, 2022, **43**(2), 519–525.
58 C. Cai, B. Liu, K. Liu, P. Li, J. Fu, Y. Wang, W. Li, C. Tian, Y. Kang and A. Stefancu, Heteroatoms induce localization of the electric field and promote a wide potential-window selectivity towards CO in the CO2 electroreduction, *Angew. Chem.*, 2022, **134**(44), e202212640.
59 A. Limaye, D. Suvlu and A. P. Willard, Water molecules mute the dependence of the double-layer potential profile on ionic strength, *Faraday Discuss.*, 2024, **249**, 267–288.
60 L. Scalfi, M. Salanne and B. Rotenberg, Molecular Simulation of Electrode-Solution Interfaces, *Annu. Rev. Phys. Chem.*, 2021, **72**, 189–212.
61 A. M. Limaye, W. Ding and A. P. Willard, Understanding attenuated solvent reorganization energies near electrode interfaces, *J. Chem. Phys.*, 2020, **152**, 11.
62 S. Baldelli, Interfacial Structure of Room-Temperature Ionic Liquids at the Solid–Liquid Interface as Probed by Sum Frequency Generation Spectroscopy, *J. Phys. Chem. Lett.*, 2012, **4**, 244–252.
63 A. W. Adamson and A. P. Gast, *Physical chemistry of surfaces*, Interscience publishers New York, 1967, vol. 150.
64 H.-J. Butt; K. Graf and M. Kappl, *Physics and chemistry of interfaces*, John Wiley & Sons, 2023.
65 M. V. Fedorov and A. A. Kornyshev, Ionic liquid near a charged wall: structure and capacitance of electrical double layer, *J. Phys. Chem. B*, 2009, **113**(13), 4500.
66 O. J. Lanning and P. A. Madden, Screening at a charged surface by a molten salt, *J. Phys. Chem. B*, 2004, **108**(30), 11069–11072.
67 D. Hubbard and R. G. Goldman, Heterogeneous Equilibria at the Glass Electrode-Solution, *J. Res. Natl. Bur. Stand.*, 1952, **48**(6), 428.
68 A. M. El-Kazzaz, *Contact charging of insulators by liquid metals*, The University of Manchester, United Kingdom, 1985.
69 M. Matsui, N. Murasaki, K. Fujibayashi, P. Y. Bao and Y. Kishimoto, Electrification of pure water flowing down a trough set up with a resin sheet, *J. Electrost.*, 1993, **31**(1), 1–10.
70 K. Yatsuzuka, Y. Mizuno and K. Asano, Electrification phenomena of pure water droplets dripping and sliding on a polymer surface, *J. Electrost.*, 1994, **32**(2), 157–171.
71 Y. Wei, X. Li, Y. Gu, L. Ding, X. Gao, Z. Zhang, C. Kvarnström, J. Bobacka, A. Ivaska, Z.-Q. Tian, Z. L. Wang and D. Wei, Probing electrical double layer via triboelectric charge transfer, *Nat. Commun.*, 2025, **17**(1), 402.
72 X. Li, Z. L. Wang and D. Wei, Iontronic logic control driven by dynamic electrical double layer regulation, *Iontronics*, 2025, **1**(1), 2.
73 X. Li, R. Li, S. Li, Z. L. Wang and D. Wei, Triboiontronics with temporal control of electrical double layer formation, *Nat. Commun.*, 2024, **15**(1), 6182.
74 X. Li, Z. L. Wang and D. Wei, Scavenging Energy and Information through Dynamically Regulating the Electrical Double Layer, *Adv. Funct. Mater.*, 2024, **34**(42), 2405520.
75 L. S. McCarty and G. M. Whitesides, Electrostatic Charging Due to Separation of Ions at Interfaces: Contact Electrification of Ionic Electrets, *Angew. Chem., Int. Ed.*, 2008, **47**(12), 2188–2207.
76 L. Bousse, N. F. D. Rooij and P. Bergveld, Operation of chemically sensitive field-effect sensors as a function of the insulator-electrolyte interface, *IEEE Trans. Electron Devices*, 1983, **30**(10), 1263–1270.

77 J. A. Davis, R. O. James and J. O. Leckie, Surface ionization and complexation at the oxide/water interface: I. Computation of electrical double layer properties in simple electrolytes, *J. Colloid Interface Sci.*, 1978, **63**(3), 480–499.
78 C. Werner, R. Zimmermann and T. Kratzmüller, Streaming potential and streaming current measurements at planar solid/liquid interfaces for simultaneous determination of zeta potential and surface conductivity, *Colloids Surf., A*, 2001, **192**(1), 205–213.
79 R. Zimmermann, S. Dukhin and C. Werner, Electrokinetic measurements reveal interfacial charge at polymer films caused by simple electrolyte ions, *J. Phys. Chem. B*, 2001, **105**(36), 8544–8549.
80 H. Kitabayashi, K. Tsuji and K. Itoh, A streaming electrification model based on differences of work function between solid materials and insulating oil, *J. Electrost.*, 2005, **63**(6–10), 735–741.
81 J. Nie, Z. Ren, L. Xu, S. Lin, F. Zhan, X. Chen and Z. L. Wang, Probing Contact-Electrification-Induced Electron and Ion Transfers at a Liquid–Solid Interface, *Adv. Mater.*, 2020, **32**(2), 1905696.
82 C. Xu, Y. Zi, A. C. Wang, H. Zou, Y. Dai, X. He, P. Wang, Y.-C. Wang, P. Feng, D. Li and Z. L. Wang, On the Electron-Transfer Mechanism in the Contact-Electrification Effect, *Adv. Mater.*, 2018, **30**(15), 1706790.
83 S. Lin, L. Xu, A. Chi Wang and Z. L. Wang, Quantifying electron-transfer in liquid-solid contact electrification and the formation of electric double-layer, *Nat. Commun.*, 2020, **11**(1), 399.
84 P. K. Panda, D. Singh, M. H. Köhler, D. D. de Vargas, Z. L. Wang and R. Ahuja, Contact electrification through interfacial charge transfer: a mechanistic viewpoint on solid–liquid interfaces, *Nanoscale Adv.*, 2022, **4**(3), 884–893.
85 H. L. Wang, L. Su, H. Y. Li, Z. L. Wang and G. Zhu, Electret-induced electric field assisted luminescence modulation for interactive visualized sensing in a non-contact mode, *Mater. Horiz.*, 2020, **7**(4), 1144–1149.
86 Z. J. Han, R. Morrow, B. K. Tay and D. McKenzie, Time-dependent electrical double layer with blocking electrode, *Appl. Phys. Lett.*, 2009, **94**, 4.
87 L. P. Block, A double layer review, *Astrophys. Space Sci.*, 1978, **55**(1), 59–83.
88 W. Xu, Y. Song, R. X. Xu and Z. Wang, Electrohydrodynamic and Hydroelectric Effects at the Water–Solid Interface: from Fundamentals to Applications, *Adv. Mater. Interfaces*, 2021, **8**(2), 2000670.
89 J. Wu, J. Cao, H. Bi, J. Zhang and Q. Cao, Liquid-solid contact electrification and its effect on the formation of electric double layer: An atomic-level investigation, *Nano Energy*, 2023, **111**, 108442.
90 X. Li, W. Tong, J. Shi, X. Zhang, Y. Chen, X. Liu and Y. Zhang, Contact-Electro-Catalysis Through Electret Behavior to Facilitate Electron Transfer, *ACS Appl. Mater. Interfaces*, 2024, **16**(32), 42293–42304.
91 C. Ye, D. Liu, Y. Gao, F. Liu, H. Xu, T. Jiang and Z. L. Wang, Electrostatic breakdown at liquid-solid-gas triple-phase interfaces owing to contact electrification, *Matter*, 2025, **8**(4), 102007.
92 X. Tao, T. Wang, L. Tan, F. Xu, A. Chen, Y. Yang, R. Zhang and X. Wang, High-Performance Constant Current Triboelectric Nanogenerator for Wind Energy Harvesting and Air Purification, *SmartSys*, 2025, **1**(4), e70012.
93 X. Li, Y. Wei, X. Gao, Z. Zhang, Z. L. Wang and D. Wei, Harnessing triboiontronic Maxwell's demon by triboelectric-induced polarization for efficient energy-information flow, *Joule*, 2025, **9**(5), 101888.
94 J. Li, J. Yin and W. Guo, Hydrovoltaic energy and intelligence: where ions meet electrons, *Iontronics*, 2025, **1**(1), 3.
95 X. Li, S. Li, X. Guo, J. Shao, Z. L. Wang and D. Wei, Triboiontronics for efficient energy and information flow, *Matter*, 2023, **6**(11), 3912–3926.
96 C.-y Liu and A. J. Bard, Electrons on dielectrics and contact electrification, *Chem. Phys. Lett.*, 2009, **480**(4), 145–156.
97 C.-y Liu and A. J. Bard, Electrostatic electrochemistry: Nylon and polyethylene systems, *Chem. Phys. Lett.*, 2010, **485**(1), 231–234.
98 J. Zhang, F. J. M. Rogers, N. Darwish, V. R. Gonçales, Y. B. Vogel, F. Wang, J. J. Gooding, M. C. R. Peiris, G. Jia, J.-P. Veder, M. L. Coote and S. Ciampi, Electrochemistry on Tribocharged Polymers Is Governed by the Stability of Surface Charges Rather than Charging Magnitude, *J. Am. Chem. Soc.*, 2019, **141**(14), 5863–5870.
99 C. Chamberlayne and R. Zare, What Role Does the Electric Double Layer Play in Redox Reactions at Planar Electrostatically Charged Insulating Surfaces?, *Top. Catal.*, 2021, 65.
100 N. Wang, W. Jiang, J. Yang, H. Feng, Y. Zheng, S. Wang, B. Li, J. Z. X. Heng, W. C. Ong, H. R. Tan, Y.-W. Zhang, D. Wang, E. Ye and Z. Li, Contact-electro-catalytic CO2 reduction from ambient air, *Nat. Commun.*, 2024, **15**(1), 5913.
101 N. Wang, W. Jiang, H. Feng, J. Yang, B. Li, T. Yu, C. Du, J. Wang, J. Z. X. Heng, J. H. Pan, Y.-W. Zhang, D. Wang, E. Ye and Z. Li, Target High-Efficient Ethylene Production from Dilute CO2 Enabled by Sustainable Contact Electrons, *Small*, 2025, **21**(13), 2411815.
102 Y.-J. Kim, Z.-Y. Huo, X. Wang, H. Dai, D.-M. Lee, I.-Y. Suh, J.-H. Hwang, Y. Chung, H. Y. Lee, Y. Du, W. Ding and S.-W. Kim, Walking-induced electrostatic charges enable in situ electroporated disinfection in portable water bottles, *Nat. Water*, 2024, **2**(4), 360–369.
103 W. Xu, H. Zheng, Y. Liu, X. Zhou, C. Zhang, Y. Song, X. Deng, M. Leung, Z. Yang and R. X. Xu, A droplet-based electricity generator with high instantaneous power density, *Nature*, 2020, **578**(7795), 392–396.
104 H. W. Gibson, J. M. Pochan and F. Bailey, Surface analyses by a triboelectric charging technique, *Anal. Chem.*, 1979, **51**(4), 483–487.
105 Z. Ying, Y. Long, F. Yang, Y. Dong, J. Li, Z. Zhang and X. Wang, Self-powered liquid chemical sensors based on solid–liquid contact electrification, *Analyst*, 2021, **146**(5), 1656–1662.
106 P. Jiang, L. Zhang, H. Guo, C. Chen, C. Wu, S. Zhang and Z. L. Wang, Signal Output of Triboelectric Nanogenerator

at Oil–Water–Solid Multiphase Interfaces and its Application for Dual-Signal Chemical Sensing, *Adv. Mater.*, 2019, **31**(39), 1902793.

107 J. Zhang, X. Wang, L. Zhang, S. Lin, S. Ciampi and Z. L. Wang, Triboelectric Spectroscopy for In Situ Chemical Analysis of Liquids, *J. Am. Chem. Soc.*, 2024, **146**(9), 6125–6133.

108 W.-Z. Song, M. Zhang, H.-J. Qiu, C.-L. Li, T. Chen, L.-L. Jiang, M. Yu, S. Ramakrishna, Z.-L. Wang and Y.-Z. Long, Insulator polymers achieve efficient catalysis under visible light due to contact electrification, *Water Res.*, 2022, **226**, 119242.

109 M. Willatzen, L. C. Lew Yan Voon and Z. L. Wang, Quantum Theory of Contact Electrification for Fluids and Solids, *Adv. Funct. Mater.*, 2020, **30**(17), 1910461.

110 Y. Zhao, Y. Liu, Y. Wang, S. Li, Y. Liu, Z. L. Wang and P. Jiang, The process of free radical generation in contact electrification at solid-liquid interface, *Nano Energy*, 2023, **112**, 108464.

111 Z. Wu, S. Wu, L. Zhang, Z. Wu, S. Hong, B. Chen, G. Zhu and Y. Jia, Low-frequency contact-electro-catalysis driven by friction between the PTFE-coated fabric and dye solution, *J. Alloys Compd.*, 2025, **1010**, 177440.

112 Z. Wang, X. Dong, X.-F. Li, Y. Feng, S. Li, W. Tang and Z. L. Wang, A contact-electro-catalysis process for producing reactive oxygen species by ball milling of triboelectric materials, *Nat. Commun.*, 2024, **15**(1), 757.

113 S. T. Muntaha, Z. L. Wang and D. Wei, Reevaluating mechano-driven chemical reactions: Insights from ultrasonic, piezo, and contact-electro mechanisms, *Electrochim. Acta*, 2025, **544**, 147563.

114 X. Dong, Z. Wang, A. Berbille, X. Zhao, W. Tang and Z. L. Wang, Investigations on the contact-electro-catalysis under various ultrasonic conditions and using different electrification particles, *Nano Energy*, 2022, **99**, 107346.

115 Z. Wang, X. Dong, F.-J. Lv and W. Tang, A perspective on contact-electro-catalysis based on frontier molecular orbitals, *Mater. Adv.*, 2024, **5**(16), 6373–6377.

116 Y. Wang, J. Zhang, W. Zhang, J. Yao, J. Liu, H. He, C. Gu, G. Gao and X. Jin, Electrostatic Field in Contact-Electro-Catalysis Driven C–F Bond Cleavage of Perfluoroalkyl Substances, *Angew. Chem., Int. Ed.*, 2024, **63**(19), e202402440.

117 W. Li, J. Sun, M. Wang, J. Xu, Y. Wang, L. Yang, R. Yan, H. He, S. Wang, W.-Q. Deng, Z.-Q. Tian and F. R. Fan, Contact-Electro-Catalysis for Direct Oxidation of Methane under Ambient Conditions, *Angew. Chem., Int. Ed.*, 2024, **63**(20), e202403114.

118 H. Jiang, F. Yang, R. Wang, G. Zhu and Y. Zhao, Synergistic contact-electro-catalysis using independent plastic types for emerging contaminants removal and resource valorization, *Chem. Eng. Sci.*, 2026, **323**, 123240.

119 A. Berbille, X.-F. Li, Y. Su, S. Li, X. Zhao, L. Zhu and Z. L. Wang, Mechanism for Generating H2O2 at Water-Solid Interface by Contact-Electrification, *Adv. Mater.*, 2023, **35**(46), 2304387.

120 Y. Shao, Y. Wei, J. Wu, W. Li, L. Huang and Y. Shi, Ultrasound-driven formation of defects and radicals in contact-electro-catalysis: a DFT and AIMD investigation, *Appl. Surf. Sci.*, 2026, **720**, 165310.

121 Z. Wang, X. Dong, W. Tang and Z. L. Wang, Contact-electro-catalysis (CEC), *Chem. Soc. Rev.*, 2024, **53**(9), 4349–4373.

122 S. Lin, X. Chen and Z. L. Wang, Contact electrification at the liquid–solid interface, *Chem. Rev.*, 2021, **122**(5), 5209–5232.

123 Y. Su, A. Berbille, X.-F. Li, J. Zhang, M. PourhosseiniAsl, H. Li, Z. Liu, S. Li, J. Liu, L. Zhu and Z. L. Wang, Reduction of precious metal ions in aqueous solutions by contact-electro-catalysis, *Nat. Commun.*, 2024, **15**(1), 4196.

124 H. Yan, X. Song, S. Li, J. Li, J. Zhang, Y. Zhang and L. Zhang, Contact-Electro-Catalysis Enables Ultrasonic Synthesis of Gold Nanoparticles at Water–PTFE Interfaces, *ChemNanoMat*, 2025, **11**(5), e202500050.

125 D. Ma, J. Zhang, W. Li, J. Ma, K. He, K. Yang, J. Cui, Q. Liu, S. Lv, M. Zhang, F. Cheng and D. Xing, FeIII-driven self-cycled Fenton via contact-electro-catalysis for water purification. npj Clean, *Water*, 2025, **8**(1), 42.

126 C. Xue, Y. Peng, Z. Fang, Y. Jiang and K. Du, Efficient degradation of metronidazole by peroxodisulfate through triboelectric effect of water eddy: Electrocatalytic promotion of Fe3 +/Fe2+ cycling, *Chem. Eng. J.*, 2025, **510**, 161705.

127 Z. Zhou, S. Zhang, D. Song, J. Cao, Y. Qiu, C. Xue, H. Xu and J. Mei, Plasmonic silver particles reduced by contact-electro-catalysis with acoustic-solid interaction mechanism for enhancing SERS detection, *J. Environ. Chem. Eng.*, 2025, **13**(6), 120102.

128 M. Shah, S. Li, Z. Yang, J. Liu, P. Peng, H. Qian, Z. L. Wang and D. Wei, Synergistic effects in triboelectric charge-driven redox reactions, *Nano Energy*, 2025, **144**, 111380.

129 Z. Liang, W. Li, J. Tu and F. R. Fan, Mechanically Induced Contact-Electro-Catalysis: Free Radical Generation, Reaction Pathways, and Catalytic Applications, *ChemCatChem*, 2025, **17**(11), e202500282.

130 X. Li and W. Tong, Contact-electro-catalysis under natural and industrial conditions: mechanisms, strategies, and challenges, *J. Mater. Chem. A*, 2024, **12**(31), 19783–19805.

131 F. Chen, J. Wu, D. Wang, Y. Xia, Q. Song, Y. Liang, P. Wang, B. Chen, Y. Liang, Y. Yin, Y. Wang, M. Song and G. Jiang, Simultaneous generation of hydroxyl and hydrogen radicals from H+/OH– pairs caused by water–solid contact electrification, *Chem. Sci.*, 2024, **15**(46), 19583–19587.

132 Y. Lai, K. Li, S. Lin, L. Zhou, Z. Yu and Y. Yuan, Contact-electro-catalysis triggers peroxymonosulfate activation for micropollutant degradation, *Sci. China: Technol. Sci.*, 2025, **68**(7), 1720502.

133 X. Zhao, Y. Su, A. Berbille, Z. L. Wang and W. Tang, Degradation of methyl orange by dielectric films based on contact-electro-catalysis, *Nanoscale*, 2023, **15**(13), 6243–6251.

134 C. Liu, L. Zhao, J. Li, J. Wang, H. Xu, X. Chen, J. Qi, C. Sun, Z. Zhu and Y. Wang, Peroxymonosulfate activation by low-

cost modified rubber during contact electrification for antibiotics efficient degradation at circumneutral pH: mechanism and toxicity assessment, *Chem. Eng. Sci.*, 2024, **285**, 119642.

135 N. Tian, J. Kuang, C. Yuan, X. Zhang, Y. Zhang and H. Huang, Direct hydrogen production from pure water through contact-electro-catalysis, *J. Mater. Chem. A*, 2025, **13**(38), 32344–32350.

136 K. Li, Y. Lai, S. Lin, L. Zhou, M. He, H. Lin and Y. Yuan, Contact-Electro-Catalysis for the Degradation of Pentachlorophenol Using Inert Fluorinated Ethylene Propylene Powders, *ACS ES&T Eng.*, 2024, **4**(10), 2485–2494.

137 D. R. Lide, *CRC handbook of chemistry and physics: a ready-reference book of chemical and physical data*, CRC press, 1995.

138 Y. Wang, P. Wei, Z. Shen, C. Wang, J. Ding, W. Zhang, X. Jin, C. D. Vecitis and G. Gao, O2-Independent H2O2 Production via Water–Polymer Contact Electrification, *Environ. Sci. Technol.*, 2024, **58**(1), 925–934.

139 H. Zou, Y. Zhang, L. Guo, P. Wang, X. He, G. Dai, H. Zheng, C. Chen, A. C. Wang, C. Xu and Z. L. Wang, Quantifying the triboelectric series, *Nat. Commun.*, 2019, **10**(1), 1427.

140 S. Li, J. Nie, Y. Shi, X. Tao, F. Wang, J. Tian, S. Lin, X. Chen and Z. L. Wang, Contributions of Different Functional Groups to Contact Electrification of Polymers, *Adv. Mater.*, 2020, **32**(25), 2001307.

141 S. Lin, M. Zheng, J. Luo and Z. L. Wang, Effects of Surface Functional Groups on Electron Transfer at Liquid–Solid Interfacial Contact Electrification, *ACS Nano*, 2020, **14**(8), 10733–10741.

142 Z.-H. Loh, G. Doumy, C. Arnold, L. Kjellsson, S. H. Southworth, A. Al Haddad, Y. Kumagai, M.-F. Tu, P. J. Ho, A. M. March, R. D. Schaller, M. S. Bin Mohd Yusof, T. Debnath, M. Simon, R. Welsch, L. Inhester, K. Khalili, K. Nanda, A. I. Krylov, S. Moeller, G. Coslovich, J. Koralek, M. P. Minitti, W. F. Schlotter, J.-E. Rubensson, R. Santra and L. Young, Observation of the fastest chemical processes in the radiolysis of water, *Science*, 2020, **367**(6474), 179–182.

143 Y. Gauduel, S. Pommeret, A. Migus and A. Antonetti, Some evidence of ultrafast H2O + -water molecule reaction in femtosecond photoionization of pure liquid water: Influence on geminate pair recombination dynamics, *Chem. Phys.*, 1990, **149**(1), 1–10.

144 F. Zhan, A. C. Wang, L. Xu, S. Lin, J. Shao, X. Chen and Z. L. Wang, Electron Transfer as a Liquid Droplet Contacting a Polymer Surface, *ACS Nano*, 2020, **14**(12), 17565–17573.

145 S. Siahrostami, S. J. Villegas, A. H. Bagherzadeh Mostaghimi, S. Back, A. B. Farimani, H. Wang, K. A. Persson and J. Montoya, A Review on Challenges and Successes in Atomic-Scale Design of Catalysts for Electrochemical Synthesis of Hydrogen Peroxide, *ACS Catal.*, 2020, **10**(14), 7495–7511.

146 X. Shi, S. Back, T. M. Gill, S. Siahrostami and X. Zheng, Electrochemical Synthesis of H2O2 by Two-Electron Water Oxidation Reaction, *Chem*, 2021, **7**(1), 38–63.

147 X. Dong, Z. Wang, Y. Hou, Y. Feng, A. Berbille, H. Li, Z. L. Wang and W. Tang, Regulating Contact-Electro-Catalysis Using Polymer/Metal Janus Composite Catalysts, *J. Am. Chem. Soc.*, 2024, **146**(41), 28110–28118.

148 J. Liu, Z. Yang, S. Li, H. Qian, T. Gan, N. Wu, Z. L. Wang and D. Wei, Modular contact-electro-chemistry based on dielectrics with work function-tunable metal coatings, *Nano Energy*, 2025, **144**, 111389.

149 N. Wang, Y. Liu, E. Ye, Z. Li and D. Wang, Contact Electrification Behaviors of Solid–Liquid Interface: Regulation, Mechanisms, and Applications, *Adv. Energy Sustainability Res.*, 2023, **4**(4), 2200186.

150 Y. Jin, S. Yang, M. Sun, S. Gao, Y. Cheng, C. Wu, Z. Xu, Y. Guo, W. Xu, X. Gao, S. Wang, B. Huang and Z. Wang, How liquids charge the superhydrophobic surfaces, *Nat. Commun.*, 2024, **15**(1), 4762.

151 Y. Liu, Q. Ge, T. Wang, R. Zhang, K. Li, K. Gong, L. Xie, W. Wang, L. Wang, W. You, X. Ruan, Z. Shi, J. Han, R. Wang, H. Fu, J. Chen, C. K. Chan and L. Zhang, Strong electric field force at the air/water interface drives fast sulfate production in the atmosphere, *Chem*, 2024, **10**(1), 330–351.

152 A. M. Kol, T. Herriman, W. Salmon, G. DiLabio and M. Jackson, Long-Range Dipole Alignment of Molecules Generates Strong Local Electric Fields at Air–Water Interfaces, *ChemRxiv*, 2025, preprint, DOI: 10.26434/chemrxiv-2025-dh30c-v2.

153 S.-Y. Yang, W. Wang, J.-J. Chen, J. S. Francisco and X.-W. Liu, Probing catalyst-free hydroxyl radical generation at microbubble interfaces, *Nat. Commun.*, 2025, **16**(1), 8835.

154 E. P. Krider, Benjamin Franklin and lightning rods, *Phys. Today*, 2006, **59**(1), 42–48.

155 P. Lenard, Ueber die Electricität der Wasserfälle, *Ann. Phys.*, 1892, **282**(8), 584–636.

156 S. Lin, L. N. Y. Cao, Z. Tang and Z. L. Wang, Size-dependent charge transfer between water microdroplets, *Proc. Natl. Acad. Sci. U. S. A.*, 2023, **120**(31), e2307977120.

157 Y. Xia, J. Xu, J. Li, B. Chen, Y. Dai and R. N. Zare, Visualization of the Charging of Water Droplets Sprayed into Air, *J. Phys. Chem. A*, 2024, **128**(28), 5684–5690.

158 S. R. Shewchuk and J. V. Iribarne, Charge separation during splashing of large drops on ice, *Q. J. R. Meteorol. Soc.*, 1971, **97**(413), 272–282.

159 D. C. Blanchard, The electrification of the atmosphere by particles from bubbles in the sea, *Prog. Oceanogr.*, 1963, **1**, 73–202.

160 L. W. Zilch, J. T. Maze, J. W. Smith, G. E. Ewing and M. F. Jarrold, Charge separation in the aerodynamic breakup of micrometer-sized water droplets, *J. Phys. Chem. A*, 2008, **112**(51), 13352–13363.

161 E. Gill, Electrification by freezing, *Br. J. Appl. Phys.*, 1953, **4**(S2), S16.

162 W. Thomson, M. Maclean and A. Galt, I. Electrification of air and other gases by bubbling through water and other liquids, *Proc. R. Soc. London*, 1985, **57**(340–346), 335–346.

163 Y. Meng, Y. Xia, J. Xu and R. N. Zare, Spraying of water microdroplets forms luminescence and causes chemical

reactions in surrounding gas, *Sci. Adv.*, 2025, **11**(11), eadt8979.
164 L. Qiu, Z. Wei, H. Nie and R. G. Cooks, Reaction Acceleration Promoted by Partial Solvation at the Gas/Solution Interface, *ChemPlusChem*, 2021, **86**(10), 1362–1365.
165 A. J. Colussi, S. Enami and S. Ishizuka, Hydronium Ion Acidity Above and Below the Interface of Aqueous Microdroplets, *ACS Earth Space Chem.*, 2021, **5**(9), 2341–2346.
166 M. Li, Y. Kan, H. Su, U. Pöschl, S. H. Parekh, M. Bonn and Y. Cheng, Spatial homogeneity of pH in aerosol microdroplets, *Chem*, 2023, **9**(4), 1036–1046.
167 E. K. Brown, G. Rovelli and K. R. Wilson, pH jump kinetics in colliding microdroplets: accelerated synthesis of azamonardine from dopamine and resorcinol, *Chem. Sci.*, 2023, **14**(23), 6430–6442.
168 M. F. Ruiz-Lopez, J. S. Francisco, M. T. C. Martins-Costa and J. M. Anglada, Molecular reactions at aqueous interfaces, *Nat. Rev. Chem.*, 2020, **4**(9), 459–475.
169 K. Y. Chan, C. Zhuang, V. G. Vuong, N. Qian, X. Gao and W. Min, Electric fields at hydrophobic water interfaces: spectroscopic evidence, physical origin, and implications on reactivity, *Chem. Soc. Rev.*, 2026, **55**, 336–357.
170 F. Wang, P. Yang, X. Tao, Y. Shi, S. Li, Z. Liu, X. Chen and Z. L. Wang, Study of Contact Electrification at Liquid-Gas Interface, *ACS Nano*, 2021, **15**(11), 18206–18213.
171 Y. Dong, S. Xu, C. Zhang, L. Zhang, D. Wang, Y. Xie, N. Luo, Y. Feng, N. Wang, M. Feng, X. Zhang, F. Zhou and Z. L. Wang, Gas-liquid two-phase flow-based triboelectric nanogenerator with ultrahigh output power, *Sci. Adv.*, 2022, **8**(48), eadd0464.
172 R. Ying, M. Ma, X. Zhao, Y. Dong, X. Zhang and Z. Gao, Ultrafast Degradation of Organic Dyes by Water Atomization and Contact-Electro-Catalysis, *Langmuir*, 2025, **41**(16), 10434–10442.
173 L. Shi, R. A. LaCour, N. Qian, J. P. Heindel, X. Lang, R. Zhao, T. Head-Gordon and W. Min, Water structure and electric fields at the interface of oil droplets, *Nature*, 2025, **640**(8057), 87–93.
174 K. Roger and B. Cabane, Why are hydrophobic/water interfaces negatively charged?, *Angew. Chem., Int. Ed.*, 2012, **51**(23), 5625.
175 L. Yang, W. Yu, X. Zeng and Y. Dai, Asymmetry in hydrophobicity induces electric potential in non-charged protein condensates, *Adv. Sci.*, 2026, e24324.
176 X. Zhao, X. Lu, Q. Zheng, L. Fang, L. Zheng, X. Chen and Z. L. Wang, Studying of contact electrification and electron transfer at liquid-liquid interface, *Nano Energy*, 2021, **87**, 106191.
177 H. Li, Z. Wang, X. Chu, Y. Zhao, G. He, Y. Hu, Y. Liu, Z. L. Wang and P. Jiang, Free Radicals Generated in Perfluorocarbon–Water (Liquid–Liquid) Interfacial Contact Electrification and Their Application in Cancer Therapy, *J. Am. Chem. Soc.*, 2024, **146**(17), 12087–12099.
178 H. Li, A. Xie, C. Hong, Z. Wang, X. Chu, Z. L. Wang, Y. Liu and P. Jiang, Hydroxyl radical generation from H2O2via liquid–liquid contact-electro-catalysis, *Chem. Sci.*, 2025, **16**(43), 20580–20593.
179 R. W. Carpick, G.-y Liu and J. C. Hemminger, At the Cutting Edge of Surface Science: A Tribute to Miquel B. Salmeron, *J. Phys. Chem. B*, 2018, **122**(2), 399–400.
180 C. J. Chen and E. R. Williams, An Alternative Explanation for Ions Put Forth as Evidence for Abundant Hydroxyl Radicals Formed Due to the Intrinsic Electric Field at the Surface of Water Droplets, *Anal. Chem.*, 2025, **97**(32), 17687–17695.
181 M. A. Eatoo and H. Mishra, Busting the myth of spontaneous formation of H2O2 at the air–water interface: contributions of the liquid–solid interface and dissolved oxygen exposed, *Chem. Sci.*, 2024, **15**(9), 3093–3103.
182 G. Rovelli, M. I. Jacobs, M. D. Willis, R. J. Rapf, A. M. Prophet and K. R. Wilson, A critical analysis of electrospray techniques for the determination of accelerated rates and mechanisms of chemical reactions in droplets, *Chem. Sci.*, 2020, **11**(48), 13026–13043.
183 A. Gray-Weale and J. K. Beattie, An explanation for the charge on water's surface, *Phys. Chem. Chem. Phys.*, 2009, **11**(46), 10994–11005.
184 S. Strazdaite, J. Versluis and H. J. Bakker, Water orientation at hydrophobic interfaces, *J. Chem. Phys.*, 2015, **143**, 8.
185 J. K. Beattie and A. M. Djerdjev, The pristine oil/water interface: Surfactant-free hydroxide-charged emulsions, *Angew. Chem., Int. Ed.*, 2004, **43**(27), 3568–3571.
186 Z. Tang, S. Lin and Z. L. Wang, Unveiling Contact-Electrification Effect on Interfacial Water Oscillation, *Adv. Mater.*, 2024, **36**(44), 2407507.
187 H. Luo; S. Gao; H. Yang; G. Wang; J. Shen; Q. Liu; J. Liu; Q. Li and P. Yang, *Contact-Electro-Catalytic Co 2 Reduction Via Solid–Liquid-Gas Interfaces Involving Liquid Metals*.
188 K. Shi, H. Meng, J. Liu, S. Ma and W. Tang, Synergistic Contact-Electro-Catalysis and Photocatalysis via TiO2@ PTFE Composites for Efficient N2 to NH3 Conversion, *Angew. Chem.*, 2025, e202515707.
189 S. Huang, Y. Liu, L. Ren, L. Huang, J. Tang, Z. Yu, M. Chen and S. Zhou, Direct Conversion of N2 to Nitric Acid via Contact Electrocatalysis, *ACS Sustainable Chem. Eng.*, 2025, **13**(27), 10486–10494.
190 C. C. Jin, Y. X. Cai, K. Q. Shi, J. H. Wu, B. Yang, S. S. Xia, A. Z. Hao, S. Lin, W. Zhao and C. Y. Li, Hydrophilic/Hydrophobic Composite Catalysts to Enhance Contact-Electro-Catalytic Performance of Polytetrafluoroethylene, *Small*, 2025, **21**(24), 2503004.
191 Z. L. Wang and A. C. Wang, On the origin of contact-electrification, *Mater. Today*, 2019, **30**, 34–51.
192 D. Wei, T. Lindfors, C. Kvarnström, L. Kronberg, R. Sjöholm and A. Ivaska, Electrosynthesis and characterisation of poly(N-methylaniline) in organic solvents, *J. Electroanal. Chem.*, 2005, **575**(1), 19–26.

